Modeling of the decomposition of iodine oxides aerosols (IOx) in the containment -Consequences on the understanding of volatile iodine behaviour in the containment

Loïc Bosland, Olivia Leroy

Modeling of the decomposition of iodine oxides aerosols (IOx) in the containment - Consequences on the understanding of volatile iodine behaviour in the containment

L. Bosland[1], O. Leroy[2]

Institut de Radioprotection et de Sûreté Nucléaire (IRSN), [1]PSN-RES/SAM/LETR, [2]PSN-RES/SEREX/L2EC, Cadarache BP 3 – 13115 Saint Paul Lez Durance, France

ABSTRACT

Iodine oxides aerosols (IOx) are fine aerosol particles that are formed in a reactor containment in case of severe accident. Their stability was studied under irradiation in representative conditions of the containment. Under the influence of the temperature, humidity and irradiation they are found to be unstable. Their decomposition kinetics and stability are studied in EPICUR facility thanks to the STEM, STEM2 and MIRE projects. An IOx decomposition model is set up in ASTEC-SOPHAEROS code (version 3.1). It considers the influence of the humidity, the temperature, and dose rate. Its application to the PHEBUS FPT-0/1/2/3 tests lead to (1) an improved modeling and understanding of the inorganic iodine volatility in the FPT-3 containment all along the transient and to (2) an improved modeling after the washing when the gaseous temperature increases (FPT-0 and FPT-1) and (3) before the washing when the humidity decreases (FPT-2) as long as a relevant molar gaseous iodine fraction coming (x_{I2_RCS}) from the reactor coolant system (RCS) is set up for FPT-0/1/2. A sensitivity analysis indicates that values of x_{I2_RCS} up to ≈ 30% would be needed to improve the modeling of iodine volatility before the washing for FPT-0/2. A fraction of 10% would be more appropriate for FPT-1. A complementary approach is on-going to quantify the influence of the uncertainties of each chemical model developed in ASTEC-SOPHAEROS code within the objective to identify which chemical phenomena are the most influent on iodine volatility in the PHEBUS containment.

Keywords

Iodine, iodine oxides aerosols decomposition, kinetics, severe accident, PHEBUS-FPT tests, ASTEC

Introduction

In case of severe accident, iodine is one of the main fission products (FP) contributing to the public thyroid dose. It has long been studied, mostly since Chernobyl and Fukushima accidents through national and international R&D programs within the objective to better evaluate gaseous iodine releases in the environment and protect the population. Gaseous inorganic iodine (I_2 and HOI) and organic iodides (RI compounds - R representing organic compounds like C_nH_m) are two main gaseous contributors to the dose. Inorganic iodine (I_2) can come from the reactor coolant system but can also be formed by several well-established containment phenomena: radiolytic oxidation of iodide ions in the sump [1,2,3,4], desorption from paint [5,6,7], radiolytic decomposition of iodine soluble aerosols like CsI or CdI_2 [8,9]. Organic iodides are formed in the containment by the iodine-paint interaction in the sump and in the gaseous phase [5,6,7], the radiolytic reaction of I_2 and volatile organic compounds (R)-H [10,11,12,13] and should not come from the RCS [14]. Gaseous HOI is difficult to detect and quantify and has sometimes been qualified as the iodine ghost species. Nevertheless, it should be possible to quantify its amount even though the technology developed by Keller in the 1970's [15,16,17] to selectively trap HOI from I_2 and RI has not been retained later for the PHEBUS FP project [18,19,20,21] and subsequent iodine R&D projects (ISTP, BIP/BIP-2/BIP-3, THAI/THAI-2/THAI-3, STEM, STEM2, THEMIS, ESTER). HOI might come from the circuit and might also be formed in the containment.

Inorganic iodine (mostly I_2) and organic iodides formation and decomposition were studied for several decades. It has been highlighted that, under irradiation or photolysis, I_2 and CH_3I are decomposed, leading to the formation of fine aerosols particle of iodine oxides (IOx) [22,23,24,25,26] with an average diameter < 1 µm [27,28,29]. HOI might also decompose into IOx aerosols under irradiation as this process exists under photolysis [30]. The interpretation of the PARIS [24] and PHEBUS data [31] has identified that IOx aerosols should not be stable and should decompose back into inorganic and/or organic iodides which has been confirmed recently [32]. Therefore, a broader approach was undertaken to complete the knowledge on IOx decomposition rate under irradiation and develop an adequate model for ASTEC-SOPHAEROS (version 3.1) severe accident code [33,34,35] thanks to the STEM, STEM2 and MIRE projects [36]. Then, this IOx decomposition model was added to the modeling and interpretation of PHEBUS FPT-0/1/2/3 tests. A comparison of the iodine volatility in the containment of PHEBUS-FPT tests has been performed to highlight the contribution of this new model to the iodine volatility.

1 Description of the experiments and the test conditions

The IOx aerosol decomposition tests were performed in EPICUR irradiator facility whose description has been detailed in previous papers [5,9,32]. The same preparation procedure of the coupon (quartz, epoxy paint and sand) has been employed to be irradiated in EPICUR facility and check IOx decomposition rate. IOx aerosols formation is achieved at room temperature by the reaction between O_3 and gaseous I_2 prior to the irradiation. Several dry and hydrated species can be formed: I_2O_4, I_2O_5, I_4O_9 (dry IOx) and: $I_2O_4.H_2O$, $I_2O_5.H_2O$, $I_4O_9.H_2O$, $I_2O_5.HIO_3$ (or HI_3O_8) or HIO_3 [32] (hydrated species). The main speciation depends on the temperature and humidity according to the following mechanisms (Eq. 1 to 11) [9,37,38,39,40,41,42,43,44]:

Hydration mechanisms leading to the formation of HIO_3 species:

$$5I_2O_4 + 4H_2O \leftrightarrow 8HIO_3 + I_2 \quad (Eq.1)$$

$$5I_4O_9 + 9H_2O \leftrightarrow 18HIO_3 + I_2 \quad (Eq.2)$$

$$3I_2O_5 + 3H_2O \leftrightarrow 2I_2O_5 - HIO_3 + 2H_2O \leftrightarrow 6HIO_3 \quad (if\ R.H > 40-60\%) \quad (Eq.3)$$

$$I_2O_5 + H_2O \leftrightarrow 2HIO_3 \quad (Eq.4)$$

Conversion mechanisms due to the effect of the temperature:

$$5I_2O_4 \leftrightarrow 4\,I_2O_5 + I_2 \quad 85-100°C < T < 130°C \quad (Eq.5)$$

$$4I_4O_9 \leftrightarrow 6\,I_2O_5 + 2I_2 + 3O_2 \quad 75-85°C < T < 125°C \quad (Eq.6)$$

$$5I_4O_9 \leftrightarrow 9\,I_2O_5 + I_2 \quad 142°C < T < 190°C \quad (Eq.7)$$

$$2I_2O_6 \leftrightarrow 2I_2O_5 + O_2 \quad 130°C < T < 170°C \quad (Eq.8)$$

$$2I_2O_5 \leftrightarrow 2I_2 + 5\,O_2 \quad 280°C < T < 350°C \quad (Eq.9)$$

$$6HIO_3 \leftrightarrow 2I_2O_5.HIO_3 + 2H_2O \quad T > 70°C \quad (Eq.10)$$

$$2I_2O_5.HIO_3 \leftrightarrow 3I_2O_5 + H_2O \quad T > 200°C \quad (Eq.10\ bis)$$

$$I_2O_5 - H_2O \leftrightarrow I_2O_5 + H_2O \quad T > 200°C \quad (Eq.11)$$

All tests operating conditions and characteristics are recapped in **Table 1** and **Table 2**. Each test is performed in three phases: (1) a pre-irradiation phase (no irradiation) of some hours (1h to 20h), (2) the irradiation phase (25h to 45h) and then the post-irradiation phase (5h to 21h, no irradiation).

During the test, IOx aerosols are decomposed into volatile iodine species that are transferred to a selective trapping device (Maypack) that discriminates iodine aerosol, inorganic and organic iodine (**Fig. 1**). The kinetics formation of these gaseous species can thus be monitored on-line [8,9,32] and employed to develop a kinetics model for IOx aerosols decomposition under irradiation.

In EPICUR tests (**Table 1**), the gaseous dose rate (D_g) is close to 1 $Gy.s^{-1}$ whereas the temperature is either 80°C, either 120°C. The relative humidity (RH) has been varied (0%, 50%, 60% and 80%). It has also been checked the influence of a low content of oxygen (3% v/v), the presence of incondensable gases such as CO and H_2 that could be present in the containment atmosphere during a severe accident. The iodine concentration on the coupon is within the order of magnitude of 10^{-3} $mol.m^{-2}$, except for AER13 (IOx deposited on Epoxy paint) for which a lower concentration has been checked ($\approx 10^{-5}$ $mol.m^{-2}$) and SF3/4 for which an IOx mass was deposited on sand [9].

For modeling purposes, the raw experimental data have to be corrected to consider the missing activity balance, the knit-mesh efficiency and the activity recovered on the walls of the vessel and loop according to the procedure detailed in [5]. The uncertainties on these corrected on-line data on the Maypack are estimated at 35% for inorganic iodine and 30% for organic iodides.

2 Results and discussion

Compared to our previous papers dealing with the study of IOx behaviour in EPICUR [9,32], additional tests were performed (IOx-2, IOx-3, Gas-IOx1, Gas-IOx2 and Gas-IOx3, **Table 1**) in order to check the influence the gaseous containment composition:

- In some reactor containment, an inert atmosphere leads to a very low dioxygen content. The influence of a low O_2 content (3% v/v) on IOx aerosols decomposition was thus studied (IOx-3 test).

- Carbon monoxide (CO) can be formed in significant quantities in the containment by molten corium-concrete interaction. As CO has been reported to be oxidized by I_2O_5 [45,46,47] and leads to the formation of I_2 ($I_2O_5 + 5CO \Rightarrow I_2 + 5CO_2$), its influence on IOx aerosols decomposition has also been check (Gas-IOx1 test).

- Dihydrogen (H_2) is formed by the fuel rods degradation in significant amount and end up in the reactor containment. I_2O_5 has also been reported to react with H_2 [48]. Dihydrogen influence on IOx aerosols stability has thus been checked (Gas-IOx-2 test).

- Finally, dry conditions were also investigated (Gas-IOx3 to complete SF3 test [9]) as well as a high content of steam (RH = 80% for IOx-2) to be more representative of short-term containment conditions for which a high humidity is expected.

The influence of these parameters is discussed in the following sections. The final on-line measurements of volatilized inorganic iodine (I_2) and organic iodide (RI) and fractions are also presented in Table 3. Then, section 3 presents a modeling approach that has led to develop an IOx decomposition model that considers the influence of various parameters (temperature, humidity, irradiation).

2.1 Effect of the influence of the relative humidity

Gas-IOx3 and SF3 tests were performed without humidity. Both tests highlight a very low release from IOx decomposition, which suggests a higher IOx stability in dry conditions. The online inorganic and organic data are not shown in this paper as the raw data were found to be under the detection limit of the facility and the corrected global volatilization (estimated from the difference between the gamma counting of the coupon before/after the irradiation in **Table 3**) highlights a significant uncertainty. As a consequence, Gas-IOx3 and SF3 data were not used to set up the model.

2.2 Effect of the gaseous atmosphere composition

The effect of a low O_2 content (3% v/v, IOx-3), CO (1% v/v, Gas-IOx1) and H_2 (1% v/v, Gas-IOx2) are shown on **Fig. 2** and **Fig. 3** and are compared to the reference test AER7 at 80°C (and its reproducibility test AER10 whose data are scattered because they were close to the detection limit of the gamma-spectrometer). One difference that can be highlighted is a later start of the release of inorganic iodine in Gas-IOx1 and Gas-IOx2 after the beginning of the irradiation (≈ 10 hours).

During the irradiation, it can be concluded that there is no significant effect of a low dioxygen content, considering a late start of the irradiation in IOx-3 (5h instead of 1h for AER7). The irradiation for Gas-IOx1 and Gas-IOx2 tests starts 10h after the beginning of the test. It can be seen that for IOx3

test, as for SF4 (IOx deposited on sand, **Fig. 11**) and Gas-IOx1/Gas-IOx2 (CO and H_2 influence, **Fig. 3**) tests, the inorganic release starts about 10 h after the beginning of the irradiation whereas it starts immediately for the other tests. It has been proposed that this delay could be to the hydration process of dry IOx that could take some hours [9,38,49] but it is not consistent with AER7 and AER10 (reproducibility or AER7). It is thus possible that sand, CO and H_2 might play a role on this delay that has still to be understood and/or that an unexpected retention of gaseous inorganic iodine on the loop occurred at the beginning of the tests.

A second difference that is observed is the behaviour of the inorganic release after the end of the irradiation. Whereas its kinetics is increased for AER7, its slope is not modified for IOx-3 (Low O_2) and the release is stopped for Gas-IOx1 (CO) and Gas-IOx2 (H_2). The chemical mechanisms leading to the existence (or the absence) of a faster post-irradiation inorganic release than during the irradiation are not identified yet. It could be from the conversion of stable IOx initial species (like I_2O_5, HIO_3) into intermediate reservoir species like $IONO_2$ or $OIONO_2$ whose formation and influence has been identified in the atmosphere [50,51,52].

2.3 Effect of the temperature

As described in our previous paper [32], among all the parameters that were checked, the temperature has the most important effect on IOx decomposition as the most important releases are observed at 120°C (AER8, IOx1 and SF4, **Table 3** and **Fig. 4**). They are supposed to come from the conversion of initial IOx (I_2O_4 and I_2O_9) into I_2O_5 that leads to the formation of I_2. Another possibility is the formation of HIO_3 that could also decompose into I_2 even though no chemical mechanism has been identified yet.

The most striking effect is observed as soon as the irradiation is stopped, whatever the temperature and mostly at 120°C (IOx2, AER7, AER10 and AER8 on **Fig. 2** and **Fig. 4**): a significant increase of the inorganic release kinetics is observed after the irradiation whereas almost no release is observed before the irradiation starts. One explanation could be that a modification of the IOx aerosols speciation on the coupon occurred during the irradiation, leading to the formation of an instable IOx specie that would be quickly decomposed as soon as the irradiation is stopped.

2.4 Effect of the deposition of IOx aerosols on Epoxy painted surface

AER9 and AER13 were performed with IOx deposited on an Epoxy paint surface. The AER9 release is higher than for the reference test AER7 [32] which indicates a different release process. As mentioned in [32], IOx aerosols could have had a chemical interaction with the Epoxy paint that does not exist in case of a quartz coupon (AER7). Another possibility is that IOx did not have time to be produced in significant amount when I_2 was introduced with O_3 in the IOx manufacturing vessel, so that gaseous I_2 could have been adsorbed on the Epoxy paint [5,6, 53,63,64,65] instead of reacting with ozone. Finally, even though IOx aerosols were inert and deposited on the Epoxy paint, as soon as I_2 is produced from their decomposition, it can be adsorbed on the Epoxy paint instead of being transferred to the Maypack. For AER9 and AER13 tests, the observed release on the Maypack is similar to the release observed for iodine-paint interaction studied in previous papers [5,32] which suggests an I_2-paint interaction (before I_2 reacts with O_3 and/or after IOx decomposition). As these two tests lead to very different on-line results than the quartz coupons, they will not be considered in the modeling approach in next section as they would deserve a more complete dataset to be considered in a reliable manner.

2.5 Formation of volatile organic iodides

In all tests, small amount of organic iodides (RI) was recovered on the charcoal filter of the Maypack (< 5%). As discussed before [5,54], they might come from the radiolytic reaction between organic pollutions and gaseous inorganic iodine that has been considered and modelled in a preliminary manner [14]. Another possibility is that volatile organic compounds (R-H) might react with deposited IOx aerosols. However, there is no indication in the literature that this reaction could exist. Therefore, it was not considered in this approach.

3 Modeling of the experimental data

The experimental data were modelled with a phenomenological approach in ASTEC-SOPHAEROS severe accident code (version 3.1). The following reaction was considered to model the inorganic iodine gaseous release from the decomposition of deposited IOx aerosols:

$$I_2O_{5\_x} \xrightarrow{k_{dec}} I_{2(g)}$$ With x = gas, aero or deposited

As observed in the experimental results, a combined thermal and radiolytic decomposition is expected. The following general gaseous I_2 formation rate has thus been defined (Eq. 12 and 13):

$$\frac{d[I_2]_g}{dt} = k_{dec}.[I_2O_5]_{gas,aero} = (k_{th} + k_\gamma.D_g).[I_2O_5]_{gas,aero} \quad \text{(Eq. 12)}$$

$$\frac{d[I_2]_g}{dt} = k_{dec}.[I_2O_5]_{deposited}.\frac{S_{wall}}{V_g} = (k_{th} + k_\gamma.D_w).[I_2O_5]_{deposited}.\frac{S_{wall}}{V_g} \quad \text{(Eq. 13)}$$

With:

k_{dec} : global IOx decomposition rate (s^{-1})

k_{th} : thermal IOx decomposition rate (s^{-1})

k_γ : radiolytic IOx decomposition rate (Gy^{-1})

D_g : gaseous dose rate ($Gy.s^{-1}$)

D_w : gaseous dose rate close to the wall on which IOx are deposited ($Gy.s^{-1}$)

$[I_2O_5]_{gas,aero}$: gaseous or aerosol IOx volumic concentration ($mol.m^{-3}$)

$[I_2O_5]_{deposited}$: deposited IOx surface concentration ($mol.m^{-2}$)

S_{wall} : wall surface (m^2) on which IOx are deposited

V_g : gaseous volume (m^3)

Organic iodides (RI) are assumed to be formed by a gaseous reaction between organic pollutions and gaseous I_2 [54].

The main parameters that were considered to develop and optimize the IOx decomposition model are the dose rate, the temperature and the humidity as observed in the previous section (experimental data). It was not considered the effect of gases such as CO and H_2 or a low content of O_2 as the result of previous section did not show a significant effect of these gases on the releases on the Maypack. Even though the post-irradiation for these tests (Gas-IOx, Gas-IOx2 and IOx3) releases are not as important as for AER7, this approach should be conservative for the release of I_{2_gas} as the model will consider a post-irradiation release in the case of a reactor calculation.

3.1 Optimization of the IOx decomposition model

3.1.1 Before the irradiation: temperature effect

IOx1 test was used to optimize the thermal decomposition of IOx (k_{th}) before being exposed to irradiation. As the test starts at 120°C and the temperature is then decreased to 80°C, the influence of the temperature could be quantified. It leads to the following IOx thermal decomposition rate (whose parameters were optimized for 80 < T < 120°C and assumed to be valid out of this range):

$$k_{th} = k_{01}(T) = k_{01}(298K).e^{-\frac{E_a}{R}.(\frac{1}{T}-\frac{1}{298})} \qquad \begin{matrix} k_{01}(298K) = 3.10^{-10}\ s^{-1} \\ E_a = +93\ kJ.mol^{-1} \end{matrix} \quad \text{(Eq. 14)}$$

Fig. 5 shows the agreement between the experiment and the model.

3.1.2 During the irradiation: radiolytic decomposition rate

Tests performed at 80°C are expected to decompose IOx in a little amount as observed in IOx1 test. Even though k_{th} could have been ignored to model the radiolytic decomposition rate at 80°C, it has been considered to better evaluate the radiolytic decomposition rate k_γ in Eq (12). AER7, AER10 and IOx2 data were used to optimise k_γ and have led to an estimation of $k_\gamma = 1.10^{-6}$ Gy^{-1} (**Fig. 6**, **Fig. 7** and **Fig. 8**). We assume that this decomposition rate is not dependant on the dose rate and the thermal-hydraulics conditions. It can also be observed that, added to the thermal effect, this radiolytic rate models in a satisfying manner the inorganic releases of AER8 at 120°C (**Fig. 9**) during the irradiation.

3.1.3 Post-irradiation IOx thermal decomposition: temperature and humidity effect

The post-irradiation optimization of k_{th} (for D_g = 0 Gy.s^{-1} on **Fig. 10**, circles and squares) shows a significant effect of the relative humidity at 80°C and 120°C as the optimized rates differ by more than one order of magnitude whereas the RH is increased from 50% to 80% (80°C) and from 50% to 60% (120°C).

In order to consider this post-irradiation effect, and more generally speaking, a decreasing dose rate effect down to possibly 0 Gy.s^{-1}, k_{th} has been completed in order to consider the influence of the relative humidity between 50% and 80% as observed on **Fig. 10**. In these situations, k_{th} is expressed as follow:

$$-\ For\ RH < 50\%: \qquad k_{th} = k_{50} = \left(\frac{k_{01}(T) - k_{02}(T)}{1.03}\right).D_{g,w} + k_{02}(T) \qquad (Eq.15)$$

$$-\ For\ 50\% < RH < 80\%: \qquad k_{th} = k_{50}.\left(\frac{k_{80}}{k_{50}}\right)^{\left(\frac{RH-50}{30}\right)} \qquad (Eq.16)$$

$$-\ For\ RH > 80\%: \qquad k_{th} = k_{80} = \left(\frac{k_{01}(T) - k_{03}(T)}{1.03}\right).D_{g,w} + k_{03}(T) \qquad (Eq.17)$$

With:

- k_{50}: thermal IOx decomposition rate if RH ≤ 50% (s^{-1})
- k_{80}: thermal IOx decomposition rate if RH ≥ 80% (s^{-1})
- $k_{01}(T)$: thermal IOx decomposition rate (s^{-1}) (same as section 3.1.1)
- $k_{02}(T)$: correction made to the thermal IOx decomposition rate $k_{01}(T)$ for RH < 50% ($k_{02}(298K)$ = 1.20.10^{-7} s^{-1} and E_a = +55 kJ.mol^{-1})

- $k_{03}(T)$: correction made to the thermal IOx decomposition rate $k_{01}(T)$ for RH > 80% ($k_{03}(298K) = 9.65.10^{-4}$ s^{-1} and E_a = -128 kJ.mol^{-1})

- $D_{g,w}$: gaseous dose rate (D_g) or gaseous dose rate close to the wall (D_w) on which IOx are deposited (Gy.s^{-1})

The full lines on **Fig. 10** indicate the evolution of k_{th} for RH = 50, 60, 70 and 80% as a function of the decreasing dose rate from 1.03 Gy.s^{-1} to 0. The comparison of the modeling of the post-irradiation experimental data is shown from **Fig. 6** to **Fig. 12**. A rather good agreement is reached for all tests. The most important discrepancies are observed for IOx2 (**Fig. 8**) and IOx3 (**Fig. 12**) but should be conservative for I_{2_gas} as they lead to a more important IOx decomposition.

3.2 Extension of the thermal decomposition model to other conditions

The effect of the relative humidity could not be checked for the following situations:

- $D_{g,w}$ increases (if $\frac{dD_{g,w}}{dt} \geq 0$ in the modeling)

- $D_{g,w}$ > 1.03 Gy.s^{-1} and $D_{g,w}$ decreases (if $\frac{dD_{g,w}}{dt} < 0$ in the modeling).

For modeling scenarii for which these cases are encountered, we assumed that $k_{th} = k_{01}(T)$ (determined in section 3.1.1). In these situations, the effect of the relative humidity is thus not considered.

3.3 Formation of organic iodides (RI)

A preliminary RI radiolytic formation model has been developed and used to model RI formation. For all tests, RI formation is reproduced in a satisfactory manner for all tests (**Fig. 6** to **Fig. 12**), even though some discrepancies remain. It needs to be completed thanks to the on-going OECD-ESTER

project. On **Fig. 5** (IOx-1 thermal test), it is found some RI on the Maypack whereas there is no irradiation. This amount could be due to (1) a RI thermal formation and/or (2) a lack of efficiency of the Knitmesh filters located upstream of the charcoal filters (**Fig. 1**). In fact, the second filter stage (KM) was originally designed to trap I_2 (molecular iodine) and was set up with this objective. However, other forms of inorganic iodine might exist, like HOI and HI, for which the Knit-Mesh (KM) might not be as effective as it is for I_2 as it was not designed for other molecules than I_2. That is why that some inorganic iodine amounts could eventually be present on the charcoal filter, even though no activity is found on the last stage of the KM. Therefore, some residual quantities of inorganic iodine might also be found on the charcoal filter for all tests and might overestimate RI formation due to the irradiation.

4 Application of the IOx decomposition model to PHEBUS-FPT tests - Consequences for the understanding of volatile iodine behaviour in the containment

The phenomenology of the PHEBUS FP tests is recapped on **Fig. 13**. After injection of the FP into the containment that was insulated from the RCS (for t < 20.000 sec), the aerosols phase took place during which aerosols settle down and were drawn onto the horizontal and vertical surfaces (t < 50.000 sec). Later on, the chemistry phase started during which the elliptic floor was washed in order to transfer the deposited aerosols into the sump. However, the washing has not been efficient for FPT-2 (23%, **Table 4**) and only in a partial manner for FPT-0 (60%) whereas the mass deposited on the floor is the main contributor to the iodine mass in the containment. Complementary containment schematic views are available on **Fig. 14** and in previous papers [31,55]. The inventories and main parameters needed for the calculations are recapped in **Table 4**. The thermal-hydraulics conditions were taken into the final PHEBUS FP reports [18,19,20,21] whereas the containment dose rate has been estimated in previous work [55,56]. For all tests, the initial gaseous average dose rate peak is < 2 $Gy.s^{-1}$. Then it decreases down to a minimum of ≈ 0.3 $Gy.s^{-1}$ at the end of the tests (≈ 4 days). In a first approach, the IOx decomposition model was added to the iodine reactions list used to model iodine volatility in PHEBUS FPT-3 containment as the molar fraction of gaseous inorganic iodine coming from the reactor coolant system (x_{I2_RCS}) was quantified accurately (≈ 95%) whereas iodine aerosol contribution was ≈ 5% [21]. Even though the sump chemistry has been considered in the calculations, it will not be discussed in this paper as it has not been observed any releases to the gaseous phase all along the PHEBUS FPT tests (and assumed to be due to the high Ag/I sump ratio for FPT-0/1, the alkaline FPT-2 sump and the high x_{I2_RCS} for FPT-3 leading iodine to be significantly adsorbed/deposited on the gaseous paint/steel surfaces leading to a low iodine mass in the sump).

4.1 Modeling of inorganic iodine volatility in PHEBUS-FPT-3 containment with ASTEC-SOPHAEROS V3.1

On **Fig. 17** (left) is shown the inorganic iodine (I_2) volatility without/with considering the IOx decomposition model for FPT-3. Whereas it is underestimated by about one order of magnitude over almost the entire transient without considering it, IOx decomposition model addition leads to a significant improved modeling all over the test. On the right part of **Fig. 17** is also shown the gaseous contribution of the IOx (before nucleation into IOx aerosols). They could represent the main gaseous iodine specie quite quickly during the transient. However, there is neither indication nor experimental evidence that IOx aerosols could be trapped in the Maypack (**Fig. 1**) as the Maypack technology was

designed before IOx existence and formation was known. Before nucleation, their gaseous speciation is diverse (IO, OIO, I_2O, I_2O_2…) and evolves with the thermal and humidity conditions. If they have been trapped in the second stage of the Maypack with I_2 (which is likely as silver is used as the main trapping agent), the sum of I_2 and gaseous IOx has to be compared to the experimental data. If not, they could be trapped on the charcoal filter and contribute the RI counting (which is not considered as a likely possibility as we expect them to have been trapped on the inorganic stage of the Maypack). Another possibility is that, as the temperature design of this kind of Maypack is usually 130°C < T < 150°C, even if $IOx_{gas/aerosols}$ are trapped on the first aerosol stage, there is a high probability that they decompose into gaseous I_2 due to the temperature according to the mechanisms shown in section 1 (Eq. (5) to Eq. (10)). For the analysis of the results in the forthcoming sections, the inorganic experimental data (I_{inorg_exp}) will be compared to the modelled I_{2_gas} (justification in the discussion section 4.3).

4.2 Influence of the gaseous iodine entering the containment from the RCS for FPT-0/1/2

In a second step, this model was added to the modeling of FPT-0/1/2 (**Fig. 19**). One important initial parameter for the calculation is the molar fraction of gaseous I_2 entering the containment from the RCS (x_{I2_RCS}). The experimental data tend to show a low x_{I2_RCS} (< 4%) [18,19,20,55,57]. However, they are some significant uncertainties on this data for these three tests for two main reasons:

- The estimation of x_{I2_RCS} is based on a total sampling time in the containment that represents less than half (< 4000 sec) of the total degradation time (≈ 8000 sec) during which the FP entered into the containment. Therefore, some I_2 amount might have been missed and x_{I2_RCS} could have been underestimated in a significant manner.

- Moreover, as the Maypack is designed to trap aerosols on the first stage (**Fig. 1**), there is a possibility that gaseous inorganic iodine (supposed to be trapped downstream, on the second stage) has been adsorbed on the surfaces developed by deposited aerosols (containing silver that could trap gaseous I_2) on the first stage (illustrated on **Fig. 1**), as observed in THAI2 data for silver aerosols [58,59]. Therefore, the activity detected on the aerosols stage could have been overestimated, leading to a significant underestimation of x_{I2_RCS} for the early measurements in the transient. This assumption is supported by the total aerosol mass that entered into the containment (**Table 4**) and the comparison of an estimation of the maximum suspended aerosols surface (**Fig. 18**): it is one order of magnitude higher for FPT-0/1 (and three times higher for FPT-2) than for FPT-3 for which x_{I2_RCS} was found to

be ≈ 95% of the containment inventory (which indicates that the inorganic iodine adsorption on the aerosols surface deposited on the first FPT-3 trapping stage was insignificant). Therefore, for FPT-0/1/2, x_{I2_RCS} could have been higher than the Maypack measurements. As a result, a sensitivity analysis was made on x_{I2_RCS} for FPT-0/1/2. The values that were investigated are 2% - 10% - 30% without/with the consideration of the IOx decomposition model.

Fig. 19 shows the influence of the IOx decomposition model on inorganic iodine volatility for 2% < x_{I2_RCS} < 30% for FPT-0/1/2. On the left part of the figures, no IOx decomposition is considered. It is observed that the inorganic iodine is significantly underestimated for (1) FPT-0 all along the test, (2) for the post - (efficient) washing phase of FPT-1 and (3) the pre–(non-efficient) washing phase of FPT-2. For these three FPT-0/1/2 calculations, there is no significant effect of x_{I2_RCS} on I_{2_gas} volatility all along the transients. Moreover, it has been identified that, when the agreement is good, it is due to another reaction that mostly drives iodine volatility: decomposition of deposited iodine multicomponent aerosols (I_{aer}, whose mass represents the main iodine containment mass contribution, **Table 4**) into I_{2_gas}.

As soon as the IOx decomposition model is activated (**Fig. 19**, right), the agreement is rather good, especially for the FPT-0/1 post-washing phase (> 31h and > 70h respectively) and the FPT-2 pre-washing phase (< 45h). The reasons for this improved agreement are:

- for FPT-0/1, the increase of the gaseous temperature after the washing (**Fig. 16**) accelerates IOx decomposition rate (Eq. 15 and **Fig. 10** for which $D_{g\_FPT-0/1} < 1.03$ Gy.s^{-1}) which improves the agreement with the experimental data.

- for FPT-2, the decrease of the humidity from 65% to 50% from the beginning of the test until the washing (< 45h) (**Fig. 15**) leads to an increase of the IOx decomposition rate (Eq. 16 and **Fig. 10** for which $D_{g\_FPT-2} < 1.03$ Gy.s^{-1}) that also improves the agreement with the experimental data.

These tendencies tend to suggest that x_{I2_RCS} ≈ 30% for FPT-0/2 could be possible and more compatible with the short and long-term data than the experimental estimation (< 4%), whereas 2% ≤ x_{I2_RCS} ≤ 10% would be expected for FPT-1.

4.3 Discussion about gaseous IO_x behaviour and contribution to the Maypack

Fig. 17 tends to indicate that IO_{x_gas} could have contributed to the inorganic iodine contribution on the Maypack. It is not known if $IOx_{\_gas}$ (before they nucleate into IOx aerosols) (1) would be present in significant amount in the gaseous phase, (2) on which stage of the Maypack they would be trapped in case they are formed and (3) if they would be stable if trapped on the first aerosol stage Maypack as it is expected that the temperature design of the Maypack (130°C < < 150°C) would lead to their decomposition into gaseous inorganic iodine. It could be that, for the PHEBUS FPT-0/1/2 tests for which the total aerosol mass (composed of FP and structure material like Ag, In, Cd…) in the containment was important, $IOx_{\_gas}$ could nucleate in a faster manner than for FPT-3 (especially in the short and mid-term). In fact, as the total aerosols suspended surface in the gaseous phase is expected to be more important for FPT-0/1/2 than for FPT-3, IOx nucleation would be favoured for these three tests. To support this assumption, **Fig. 18** estimates the total estimated aerosol surface suspended in the containment for FPT-1 and FPT-3 versus the AMMD, assuming that the whole aerosol mass is suspended (before settling) and that aerosols all have the same density (S_{aer} = 6.maer/(ρ_{aer}.AMMD)). The whole aerosol surface is one order of magnitude higher for FPT-1 than for FPT-3 for each AMMD. Even though we consider AMMD = 1 µm for FPT-3 and AMMD = 4 µm fpr FPT-1, there is still a factor of 3 between the aerosol surface estimation.

As a consequence, $IOx_{\_gas}$ nucleation is expected to have been more important for FPT-0/1/2 than for FPT-3, especially during the aerosol phase and before the floor washing. As a result, the inorganic iodine counting on the FPT-3 Maypack could have also included $IOx_{\_gas}$ whereas it is less likely for FPT-0/1/2. Therefore, depending on the aerosols amount entering into the containment and the surface developed by these suspended aerosols and as I_{2_gas} can be adsorbed on this suspended surface, the quantification of x_{I2_RCS} entering the containment (and I_{2_gas} quantification) could be significantly underestimated in the short term.

5 Consequences for the understanding of the influence of x_{I2_RCS} on iodine Source Term (ST)

The development of this IOx aerosols decomposition model leads to possibly questioning the historical x_{I2_RCS} value (5% of the containment inventory as a conservative assumption [60,61,62]) in a significant manner. Considering a revised x_{I2_RCS} up to 30% would significantly question this historical approach and lead to revising the consequences for the Source Term (ST) estimation.

Nevertheless, even though a very high x_{I2_RCS} is considered (like x_{I2_RCS} = 95% for FPT-3), there are several identified phenomena whose effect is to quickly lead to a significant decrease of I_{2_gas} as observed on **Fig. 17** for PHEBUS FPT-3 (decrease of I_{2_gas} by two orders of magnitude in ≈ 10 hours):

- The adsorption of I_{2_gas} on the surface developed by the suspended aerosols (estimated to several hundreds to thousands of m² in the short term) that is expected to significantly contribute to I_{2_gas} depletion

- The adsorption of I_{2_gas} by the Epoxy paint has been shown to be an important phenomenon contributing to I_{2_gas} depletion [63,64,65,66].

- I_{2_gas} can also be decreased by its gaseous transfer into the sump. In case of spray system activation, its transfer would be facilitated [67,68,69].

- I_{2_gas} will be converted into IOx aerosols [24,27,70,71]. As they are soluble compounds, in case the spray system is activated, it should lead to an efficient transfer of suspended and deposited IOx aerosols into the sump.

Therefore, even though a high x_{I2_RCS} is reached (like FPT-3) in case of severe accident, adsorption of I_2 on surfaces (aerosols, paints and eventually steel and concrete), radiochemistry (leading to soluble IOx aerosols formation) and transfer mechanisms to the sump (by diffusiophoresis, convection and spray system) and should lead to deplete I_{2_gas} by several orders of magnitude in some hours, as observed in FPT-3 [21]. Therefore, even though x_{I2_RCS} is a parameter of prior importance in the short term for the ST evaluation in case of containment leakage, as soon as the containment chemistry will starts, x_{I2_RCS} should be a parameter whose influence on iodine volatility and ST evaluation should decrease in the long run (assuming that the releases from the core and RCS to the containment have been stopped).

6 Conclusions and perspectives

Iodine oxides aerosols decomposition has been studied under different conditions in EPICUR facility. The influence of temperature, dose rate and humidity has been studied, leading to the development of a phenomenological model in ASTEC-SOPHAEROS severe accident code. The application of this

model to the iodine volatility in PHEBUS FP tests leads to an improved modeling of the inorganic iodine volatility all over the transients which indicates that IOx decomposition is an important phenomenon that contributes to iodine volatility in a significant manner, depending on the thermal-hydraulic conditions (temperature and humidity) and the dose rate.

A sensitivity analysis on x_{I2_RCS} has led to consider that higher x_{I2_RCS} could have been possible in PHEBUS FPT-0/1/2 tests. Nevertheless, even though x_{I2_RCS} is very influent on iodine volatility in the short term, its long-term influence fades away as the containment chemistry start and takes on as soon as iodine reaches the containment. Therefore, the effect of mid- and long-term containment chemistry is to balance a possible high initial x_{I2_RCS}. A more complete analysis has been performed and published recently [72] in order to identify (1) how long does it takes to balance a high x_{I2_RCS} and (2) which kinetics parameters and which chemical reactions are the most influential on gaseous iodine volatility and evolution in PHEBUS FPT tests, considering the model uncertainties and their propagation all along the PHEBUS FPT calculations.

7 Acknowledgments

Authors acknowledge the OECD hosting the STEM and STEM2 projects as well as the French Government for MIRE project funding through the National Research Agency (ANR, grant agreement N° ANR-11-RSNR-0013-01) and the related partners of these three projects for their support:, Electricité De France (EDF), Aix-Marseille Université, Framatome, CNRS, Université de Lorraine, ARMINES, Université Lille 1, the Atomic Energy of Canada Limited (AECL), the Canadian Nuclear Laboratories (CNL), the Teknologian tutkimuskeskus VTT (Finland), Ústav Jaderného výzkumu Řež a.s (UJV, Czech Republic), The Gesellschaft für Anlagen – und Reaktorsicherheit (GRS, Germany), The Korea Atomic Energy Research Institute (KAERI), The Korea Institute for Nuclear Safety (KINS) and The US Nuclear Regulatory Commission (USNRC, USA), Nuclear Regulation Authority (NRA, Japan), Nuclear National Laboratory Limited (NNL, UK). Authors also acknowledge Juliette Colombani, Cyrille Duffieux, Laurent Martinet and Cécile Cunin for their experimental contribution.

Table 1: Experimental conditions of the IOx aerosol decomposition tests of STEM, STEM2 and MIRE projects

Project	Test name	Substrate composition	Initial Iodine concentration on the coupon (mol(I).m^{-2})	Average dose rate (Gy.s^{-1})	Pressure (absolute bar)	Temperature (°C)	R.H. during irradiation (%)	Gaseous flow (air + steam) in the vessel (L.min^{-1})	Studied parameter
STEM	AER7	Quartz	$(2.4 \pm 0.1).10^{-3}$	1.03 ± 0.10	1.65 ± 0.10	80 ± 3	50 ± 3	0.26 ± 0.01	Reference test
	AER10		$(1.8 \pm 0.1).10^{-3}$	0.86 ± 0.09	1.61 ± 0.10			0.26 ± 0.01	Reproducibility test
	AER8		$(3.7 \pm 0.2).10^{-3}$	0.92 ± 0.09	3.43 ± 0.20	120 ± 3		0.25 ± 0.01	Temperature
	AER9	Epoxy paint	$(3.2 \pm 0.1).10^{-3}$	0.94 ± 0.09	1.65 ± 0.10	80 ± 3		0.25 ± 0.01	Substrate
/	AER13		$(4.5 \pm 0.2).10^{-5}$	0.39 ± 0.04	1.66 ± 0.10			0.25 ± 0.01	Surface
STEM2	IOx-1	Quartz	$(1.9 \pm 0.1).10^{-3}$	0	3.49 ± 0.20 and then 1.67 ± 0.10	120 ± 3 and then 80 ± 3	50 ± 3	0.25 ± 0.01	Thermal decomposition
	IOx-2		$(3.0 \pm 0.2).10^{-3}$	0.75 ± 0.08	1.62 ± 0.10	80 ± 3	80 ± 3	0.26 ± 0.01	Humidity
	IOx-3		$(2.8 \pm 0.2).10^{-3}$	0.58 ± 0.06	1.60 ± 0.10		50 ± 3	0.25 ± 0.01	Low O_2 (3% v/v)
	Gas-IOx1		$(5.6 \pm 0.3).10^{-3}$	0.67 ± 0.07	1.66 ± 0.10			0.29 ± 0.01	CO effect (1% v/v)
	Gas-IOx2		$(1.5 \pm 0.2).10^{-3}$	0.53 ± 0.05	1.60 ± 0.10			0.26 ± 0.01	H_2 effect (1% v/v)
	Gas-IOx3		$(1.4 \pm 0.2).10^{-3}$	0.53 ± 0.05	1.58 ± 0.10		0	0.26 ± 0.01	Dry condition
MIRE	SF3	Sand filter	Deposited mass: m=1.1 ± 0.1 mg	0.67 ± 0.13	3.50 ± 0.10	120 ± 3	0	0.34 ± 0.01	Dry condition
	SF4		Deposited mass: m=0.98±0.09 mg	0.61 ± 0.12			60 ± 4	0.35 ± 0.01	Humidity

Table 2: Duration of the three phases of the IOx aerosols decomposition tests of STEM, STEM2 and MIRE projects

Test name	**Duration of the pre-irradiation phase (hours) (no irradiation)**	**Duration of the irradiation phase (hours)**	**Duration of the post-irradiation phase (hours) (no irradiation)**
AER7	1h (dry air)	30h (RH = 50 %)	4h (RH = 48 %)
AER10	1h (dry air) + 9h (RH = 50%)	30h (RH = 50 %)	10h (RH = 50 %) + 1h (dry air)
AER8	1h (dry air) + 8.5h (RH = 50%)	30h (RH = 50 %)	4h (RH = 50 %) + 1h (dry air)
AER9	1h (dry air)	30h (RH = 50 %)	4h (RH = 50 %) + 1h (dry air)
AER13	1h (dry air)	45h (RH = 50%)	5h (RH = 50%) + 1h (dry air)
IOx-1	20h (RH = 50%)	No irradiation	20h (RH = 50%) + 1h (dry air)
IOx-2	1h (dry air) + 9h (RH = 80%)	30h (RH = 80%)	9h (RH = 80%) + 1h (dry air)
IOx-3	1h (N_2+low O_2)+4h (RH=80%,low O_2 3% v/v)	30h (RH = 50%, low O_2)	5h (RH = 50%) + 10h (N_2 + low O_2 v/v)
Gas-IOx1	1h (CO 1%v/v + dry air) + 9h (RH = 80%)	30h (CO 1%v/v, RH=50%)	9h (CO 1%v/v + RH=80%)+1h (dry air)
Gas-IOx2	1h (H_2 1%v/v + dry air) + 9h (RH = 80%)	30h (H_2 1%v/v, RH=50%)	9h (H_2 1%v/v + RH=80%)+1h (dry air)
Gas-IOx3	10h (dry air)	30h (RH = 0%)	10h (dry air)
SF3	3h (dry air)	25h (dry air)	8h (dry air)
SF4	2h (RH = 60%)	38h (RH = 60%)	6h (RH = 60%) + 1h (dry air)

Table 3: Final corrected on-line measurements of the IOx aerosols decomposition tests (%)

Test name	Substrate composition	Studied parameter	Activity Balance (%)	Global volatilization (%)	Final corrected on-line RI (%)	Final corrected on-line I_2 (%)
AER7	Quartz	Reference test	98.0 ± 1.0	14.3 ± 0.2	1.1 ± 0.3	13.1 ± 4.6
AER10		Reproducibility test	97.8 ± 0.9	13.0 ± 0.9	0.4 ± 0.1	12.5 ± 4.4
AER8		Temperature	101.3 ± 4.2	59.3 ± 1.6	2.4 ± 0.7	58.1 ± 20.3
AER9	Epoxy paint	Substrate	97.2 ± 1.5	58.4 ± 0.7	1.4 ± 0.4	57.1 ± 20.0
AER13		Surface concentration	97.4 ± 3.3	12.9 ± 0.8	2.2 ± 0.7	10.6 ± 3.7
IOx-1	Quartz	Thermal decomposition	94.5 ± 0.5	27.0 ± 0.3	1.5 ± 0.5	24.5 ± 8.6
IOx-2		R.H	98.8 ± 3.7	7.5 ± 0.7	0.7 ± 0.2	6.8 ± 2.4
IOx-3		Low O_2 (3% v/v)	103.1 ± 4.3	3.4 ± 0.2	1.2 ± 0.4	5.3 ± 1.9
Gas-IOx1		CO effect	99.7 ± 5.8	12.0 ± 5.7	0.5 ± 0.2	11.5 ± 4.0
Gas-IOx2		H_2 effect	103.6 ± 6.9	11.2 ± 6.8	0.7 ± 0.2	14.0 ± 4.9
Gas-IOx3		Dry condition	97.0 ± 3.7	5.5 ± 3.7	0.1 ± 0.03	5.5 ± 1.9
SF3	Sand filter	Dry condition	100.0 ± 2.0	1.8 ± 2.3	0.5 ± 0.2	1.8 ± 0.6
SF4		Humidity	99.4 ± 1.2	35.0 ± 0.5	0.5 ± 0.2	33.8 ± 11.8

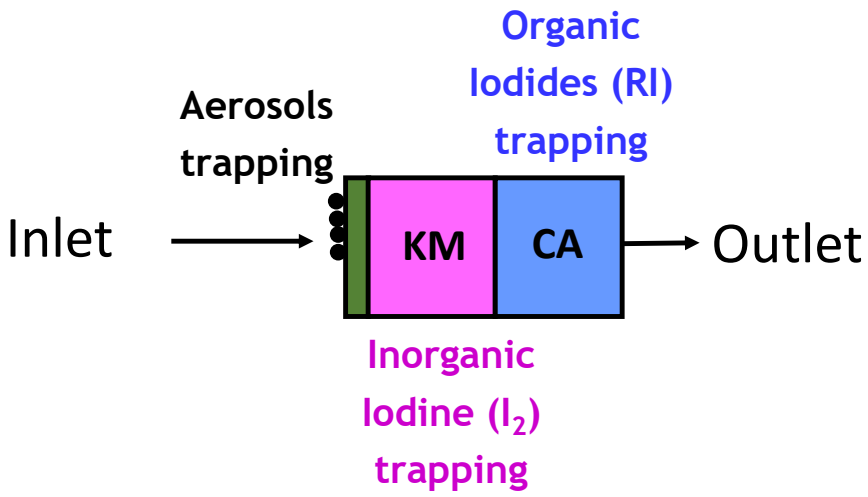

Fig. 1: schematic view of a Maypack (130°C < T < 150°C): the first stage traps aerosols, the second stage (Knitmesh, KM) traps inorganic iodine and the third stage (charcoal, CA) traps organic iodine (and small remaining inorganic iodine amount that have not been trapped on the KM)

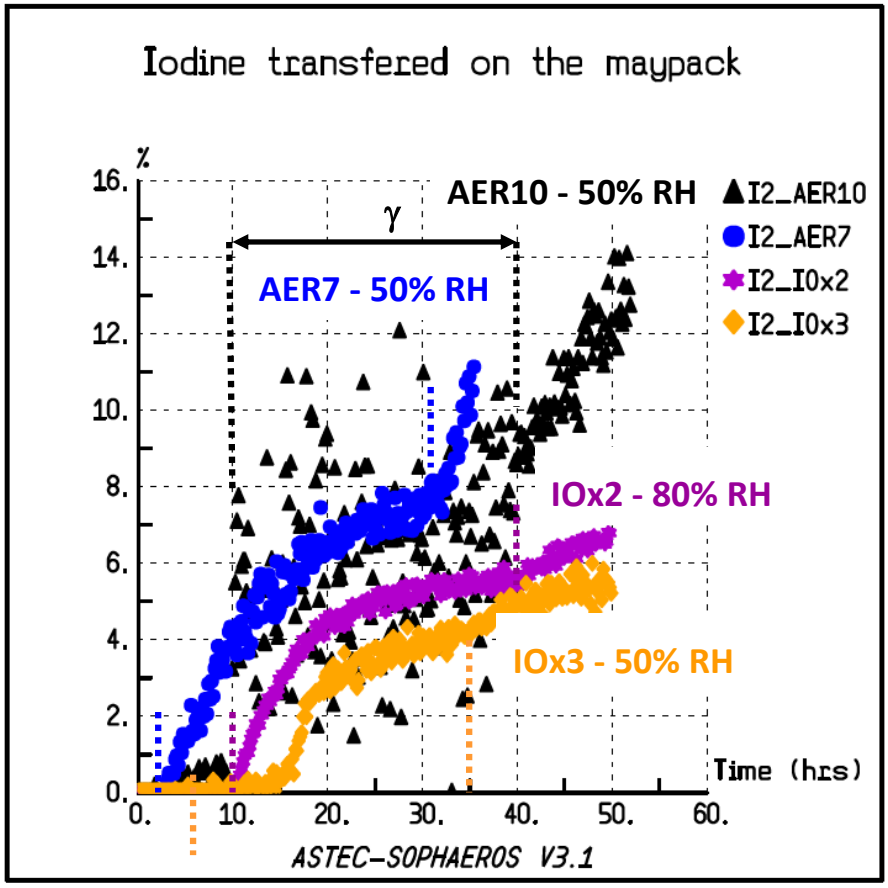

Fig. 2: Corrected inorganic release on the knit-mesh filter of the Maypack for AER7/AER10/IOx2/IOx3 tests - Decomposition of IOx aerosols deposited on a quartz coupon under irradiation at 80°C

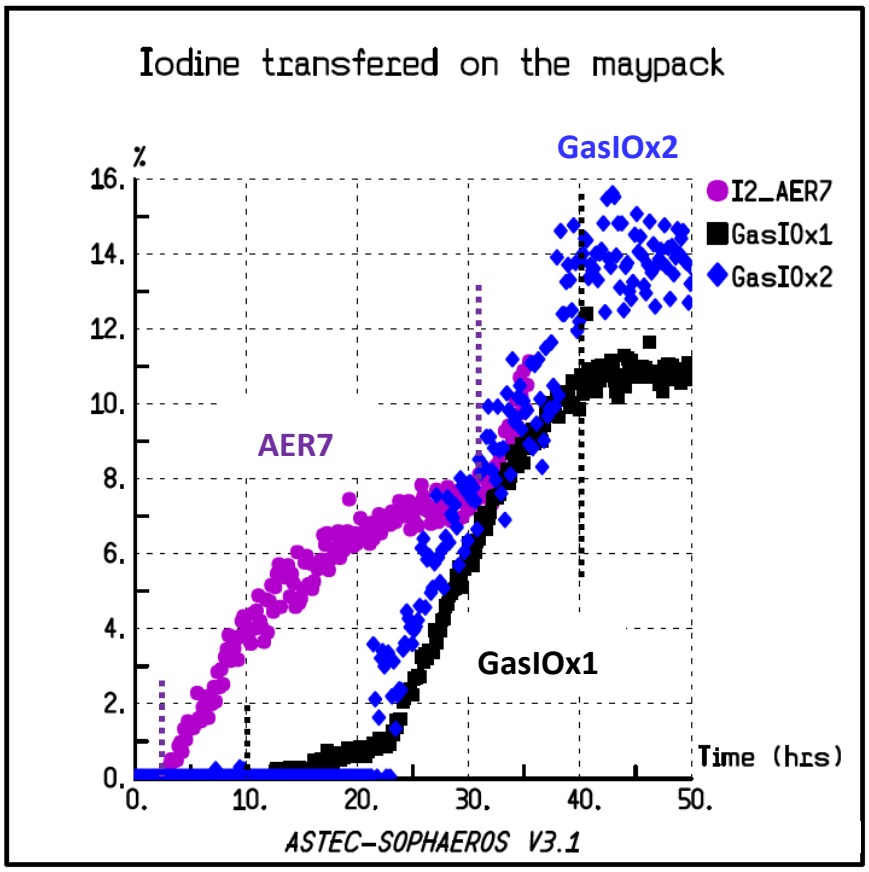

Fig. 3: Corrected inorganic release on the knit-mesh filter of the Maypack (left) for AER7/GasIOx1/GasIOx2 tests - Decomposition of IOx aerosols deposited on a quartz coupon under irradiation at 80°C

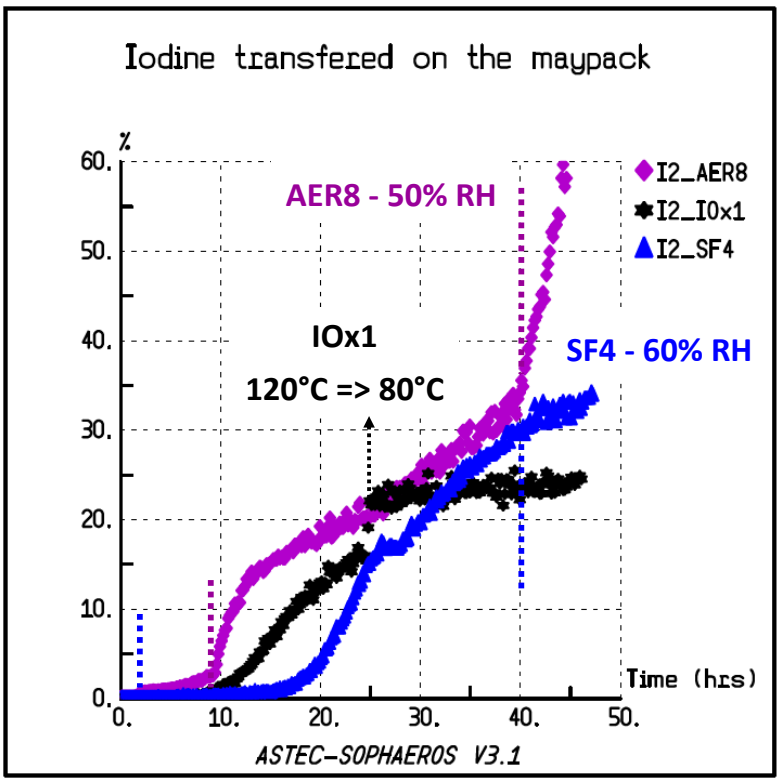

Fig. 4: Corrected inorganic release on the knit-mesh filter of the Maypack (left) for AER8/IOx1/SF4 tests at 120°C (and 80°C for the second part of IOx1 which is a test without irradiation)

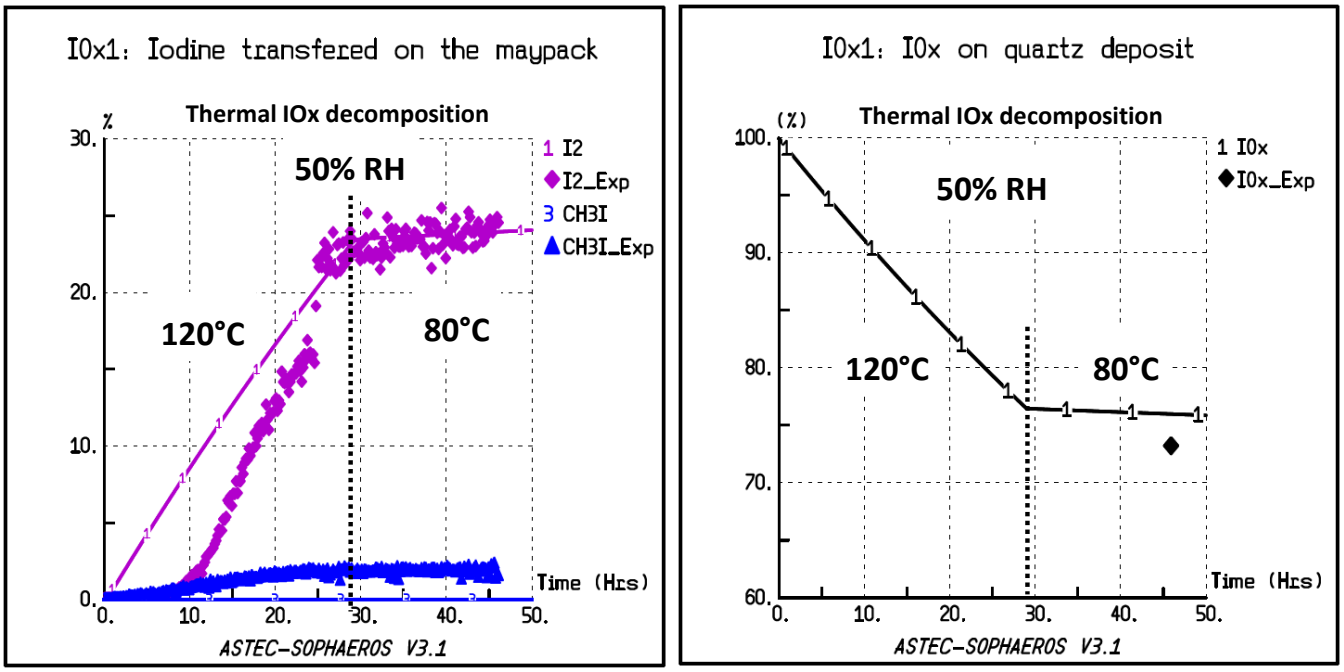

Fig. 5: Comparison of inorganic (diamond) and organic (triangle) releases on the knit-mesh filter (left) and the remaining deposited IOx amount on the coupon for IOx1 with the ASTEC modelling

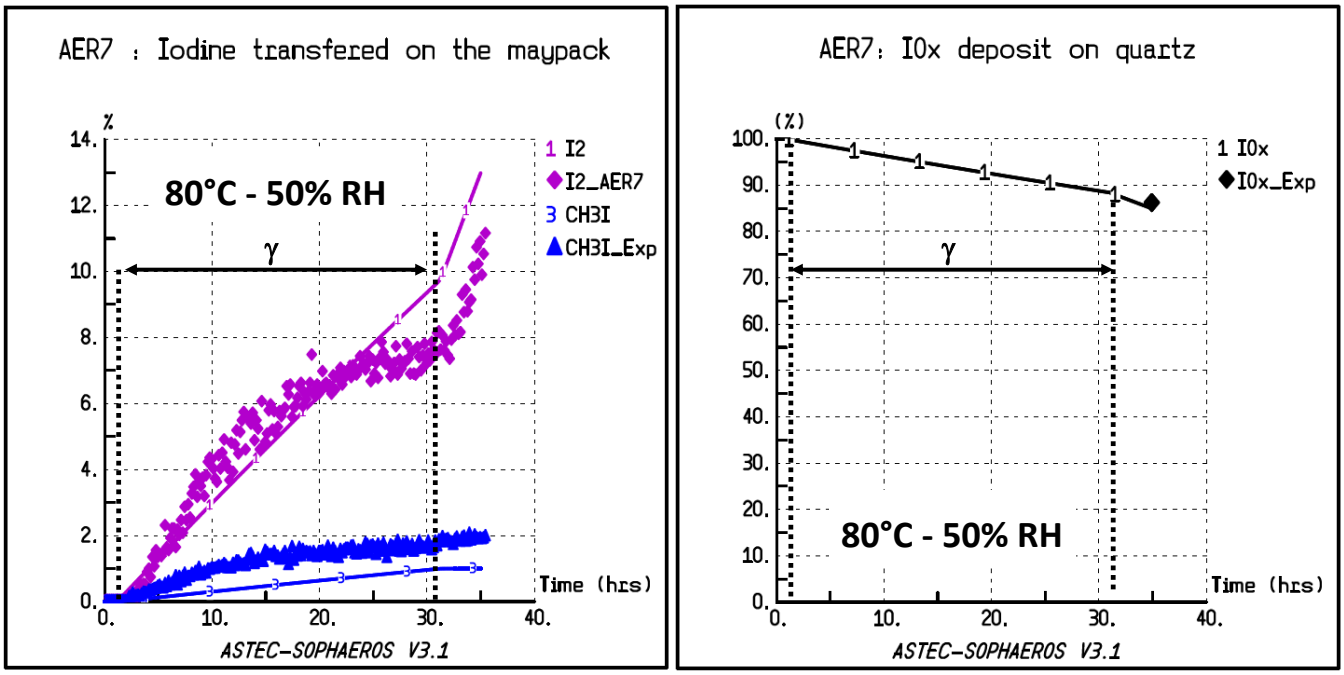

Fig. 6: Comparison of inorganic (diamond) and organic (triangle) releases on the knit-mesh filter (left) and the remaining deposited IOx amount on the coupon for AER7 with the ASTEC modelling

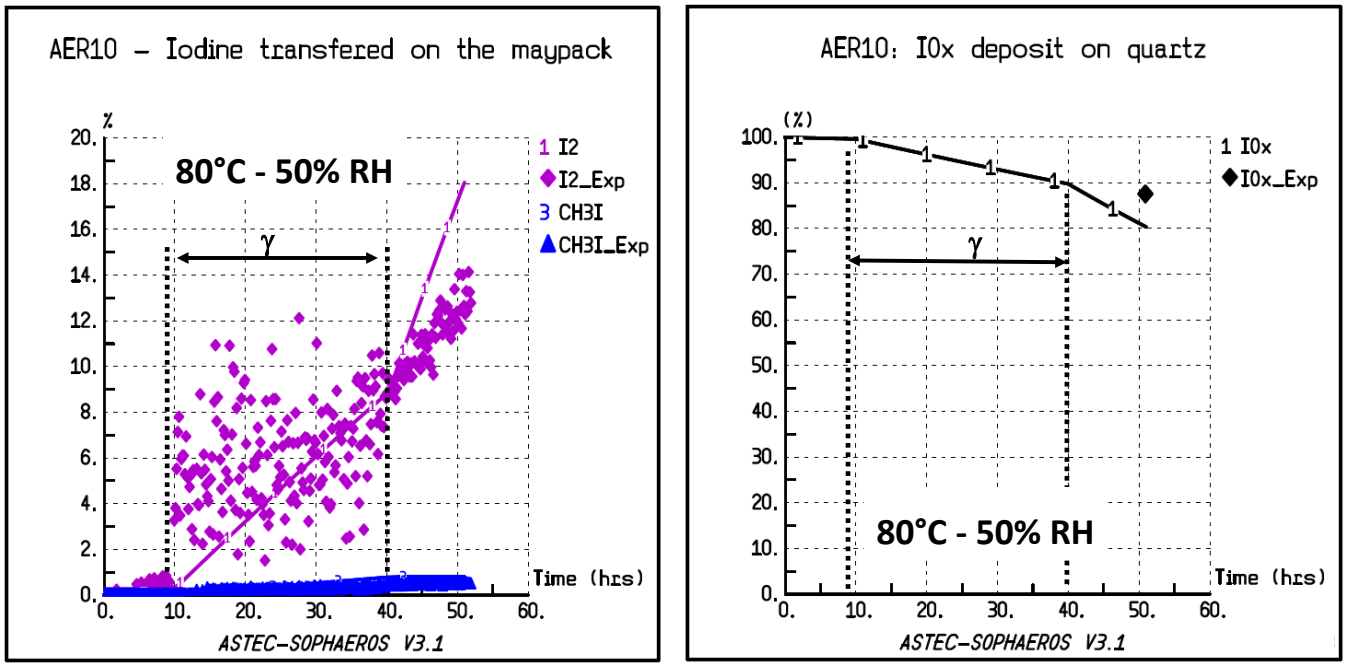

Fig. 7: Comparison of inorganic (diamond) and organic (triangle) releases on the knit-mesh filter (left) and the remaining deposited IOx amount on the coupon for AER10 with the ASTEC modelling

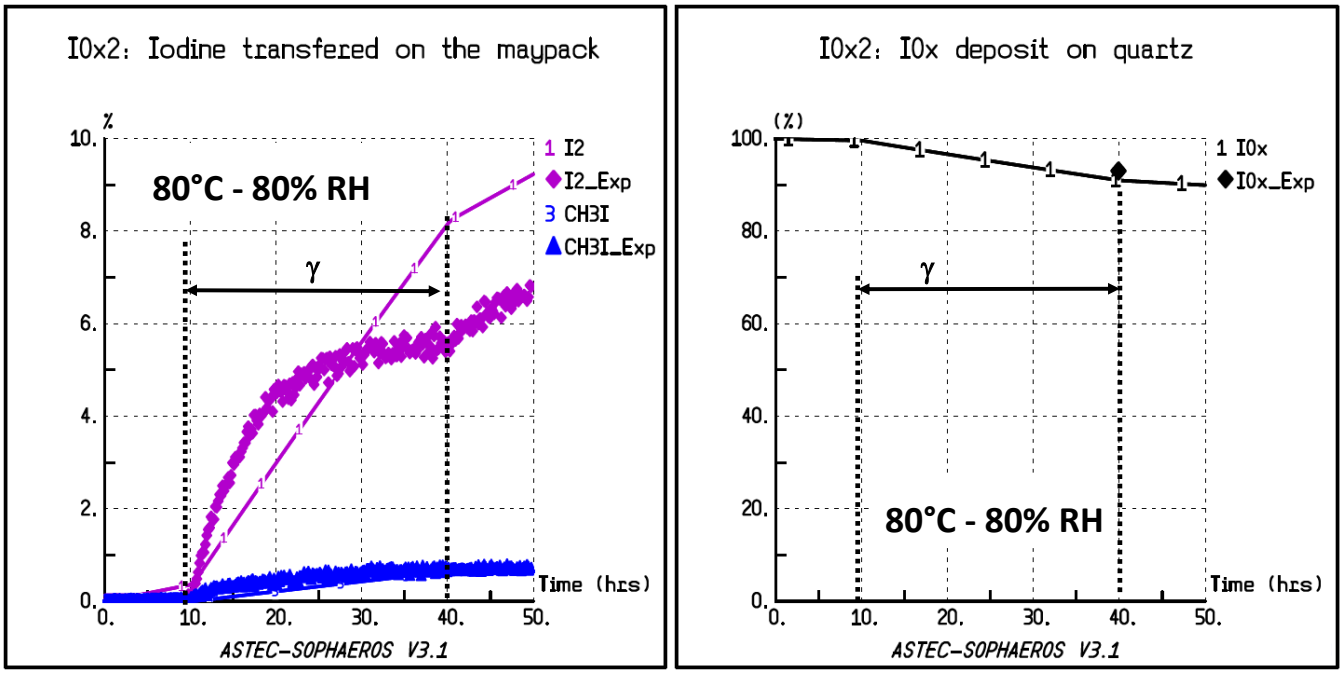

Fig. 8: Comparison of inorganic (diamond) and organic (triangle) releases on the knit-mesh filter (left) and the remaining deposited IOx amount on the coupon for IOx2 with the ASTEC modelling

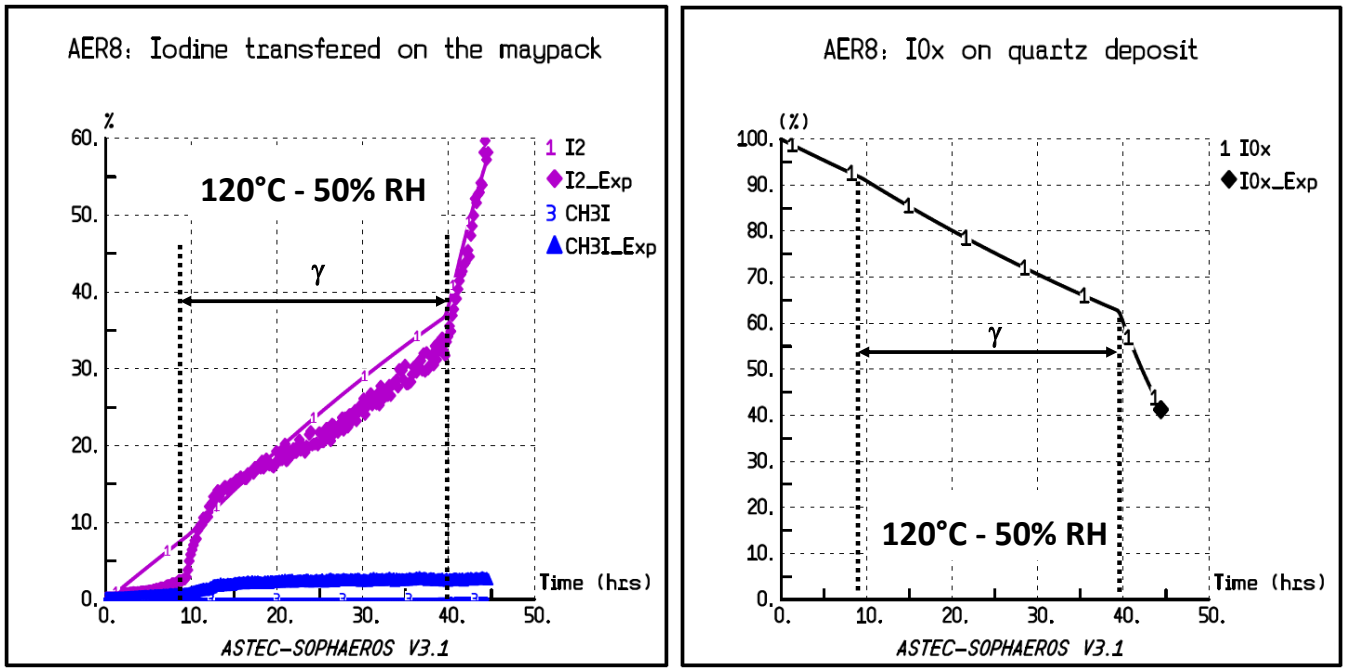

Fig. 9: Comparison of inorganic (diamond) and organic (triangle) releases on the knit-mesh filter (left) and the remaining deposited IOx amount on the coupon for AER8 with the ASTEC modelling

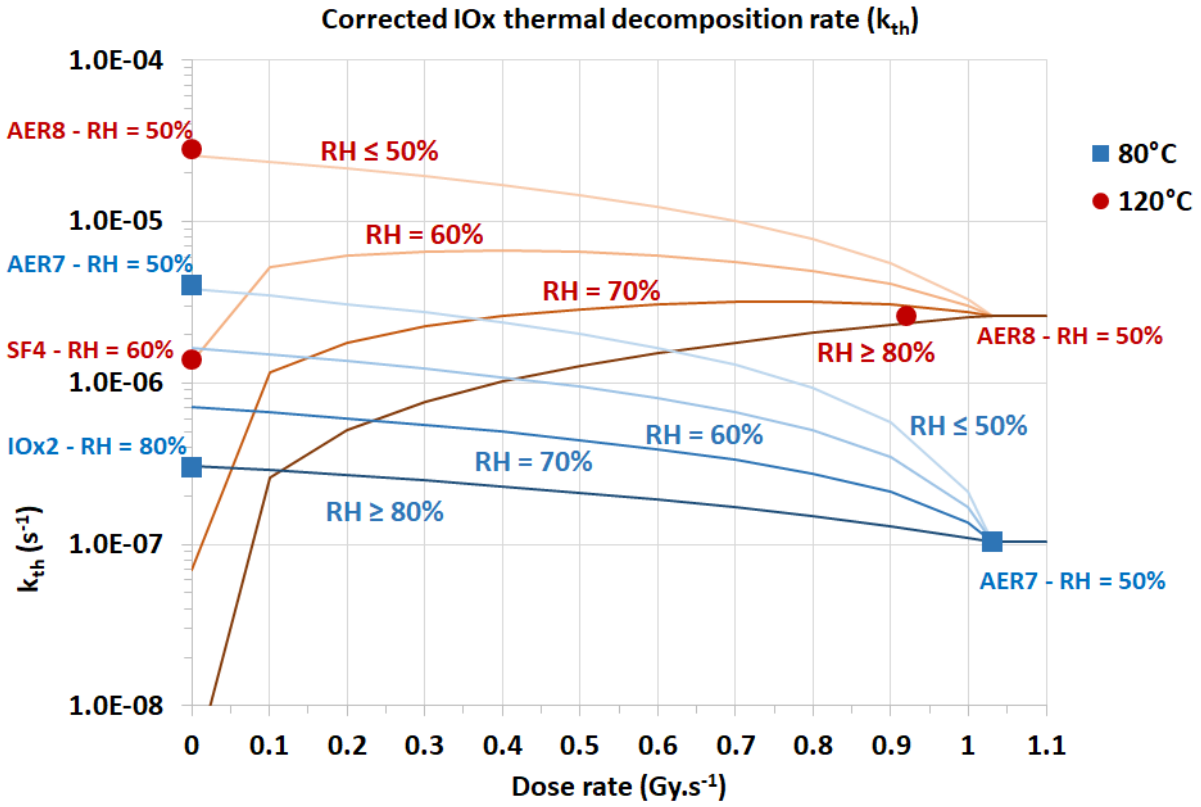

Fig. 10: Optimized (squares and circles) and extrapolated corrected IOx thermal decomposition rate (k_{th}, s^{-1}) at 80°C and 120°C (D_g = 0 addresses only post-irradiation situations on this figure)

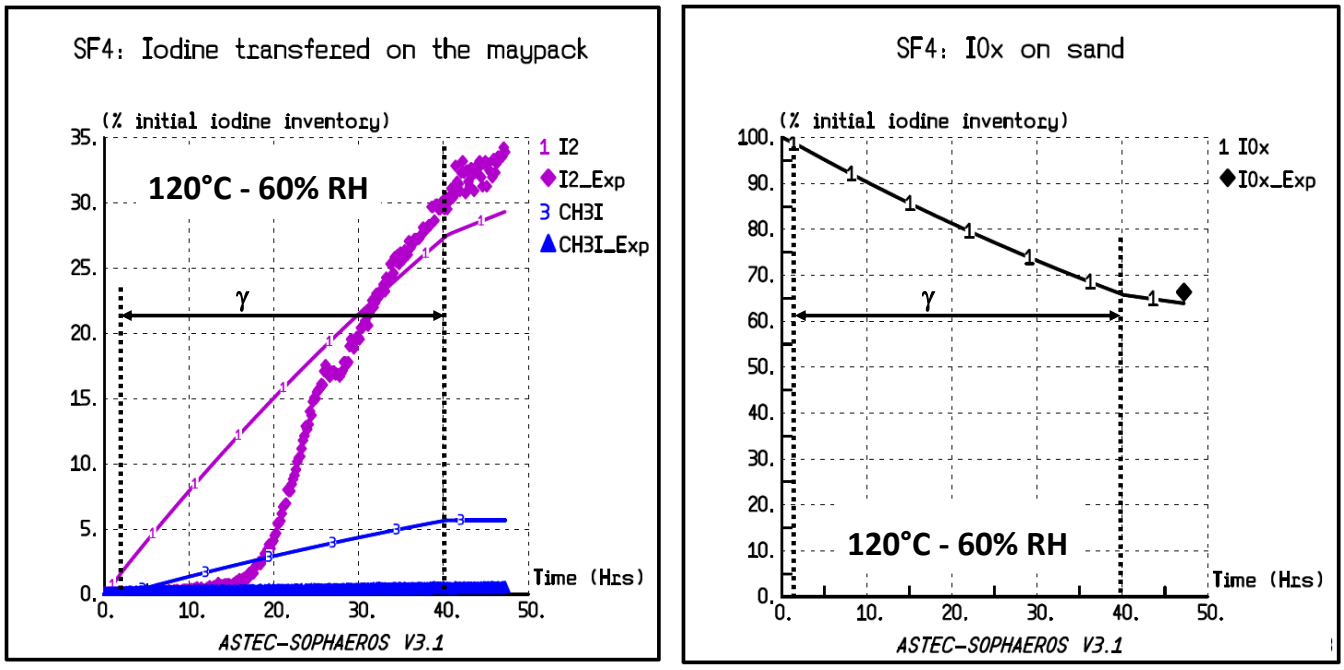

Fig. 11: Comparison of inorganic (diamond) and organic (triangle) releases on the knit-mesh filter (left) and the remaining deposited IOx amount on the coupon for SF4 with the ASTEC modelling

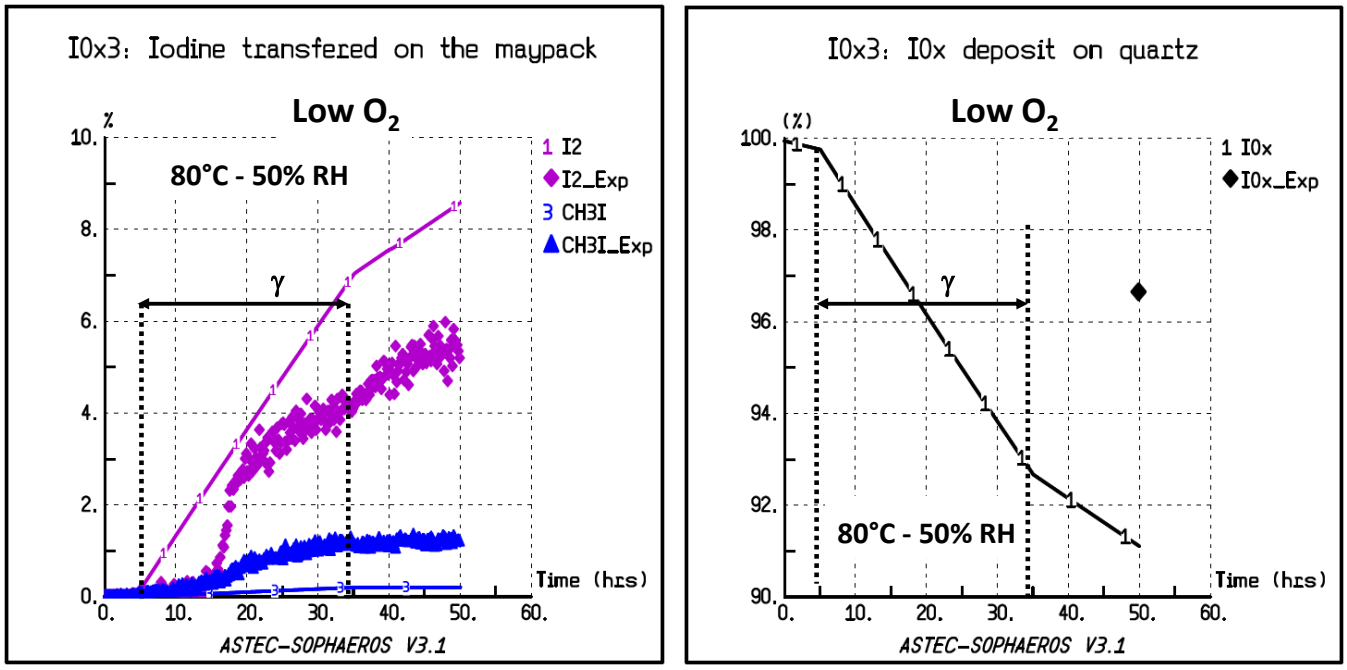

Fig. 12: Comparison of inorganic (diamond) and organic (triangle) releases on the knit-mesh filter (left) and the remaining deposited IOx amount on the coupon for IOx3 with the ASTEC modelling

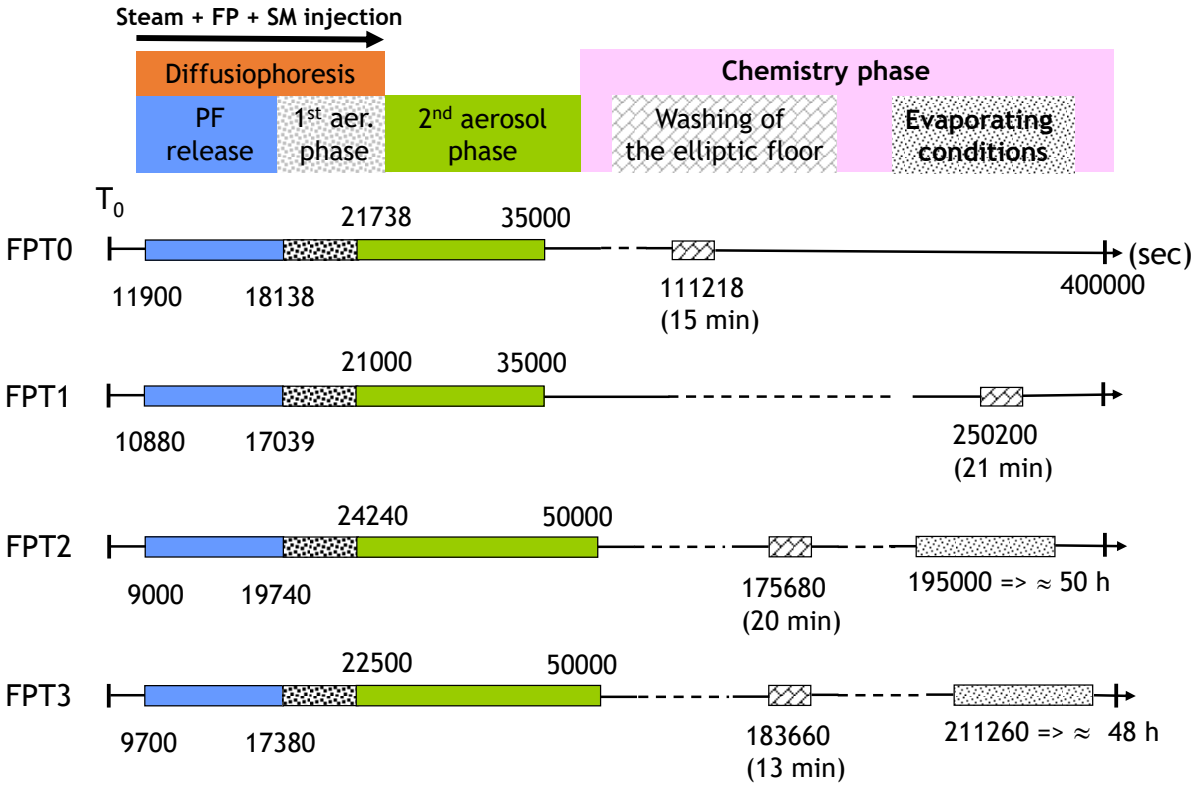

Fig. 13: Chronology of the PHEBUS FPT tests for the containment

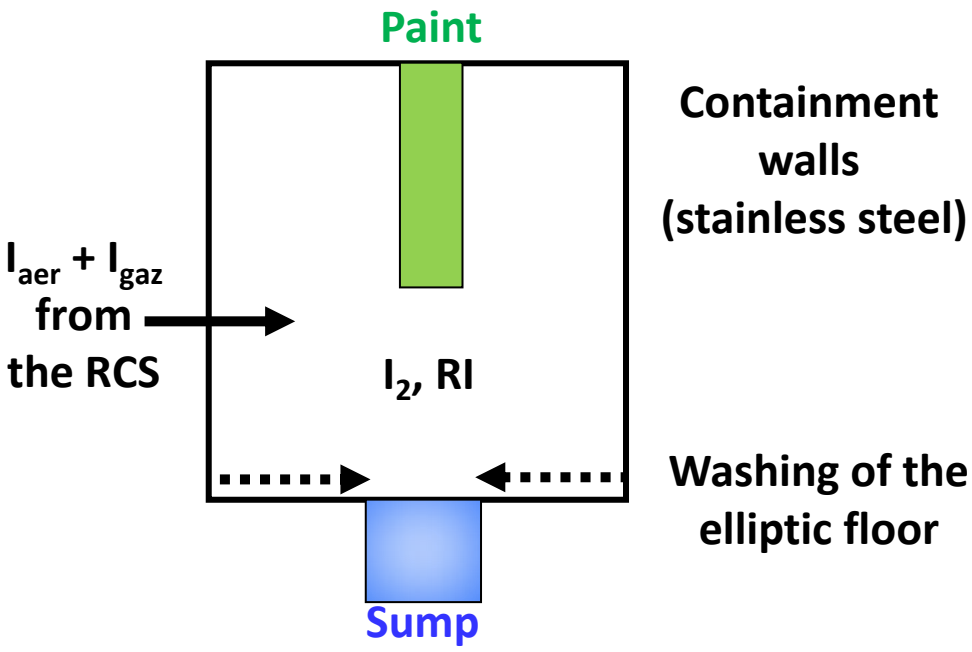

Fig. 14: schematic view of the PHEBUS containment

Table 4: Iodine inventory in the containment of PHEBUS FPT-0/1/2/3 [18,19,20,21]

	FPT-0	FPT-1	FPT-2	FPT-3
Core inventory (mg)	36	1120	1570	1190
Iodine released from the core to the containment (%)	63.8	63.8	56.4	34.1
Containment inventory (aerosol + gaseous) (mg)	23	715	885	406
Total containment aerosol mass (g) (without considering the oxygen atom contribution)	119.0	130.7	45.0	13.6
Iodine aerosol mass deposited on the elliptic floor at the end of the aerosol phase (≈ 10 hours) (mg)	12 (± 21%)	490 (± 36%)	595 (± 30%)	4 (± 17%)
Washing time (sec)	111218	250200	175680	183660
Washing duration (min)	15	21	20	13
Iodine mass (aerosols) washed into the sump by the washing (mg)	7 (± 30%) (insoluble)	450 (± 36%) (insoluble)	115 (± 20%) (46% soluble and 54% insoluble)	4
Iodine washing efficiency (%)	69	92	23 (a pump issue led to a low washing flowrate)	97

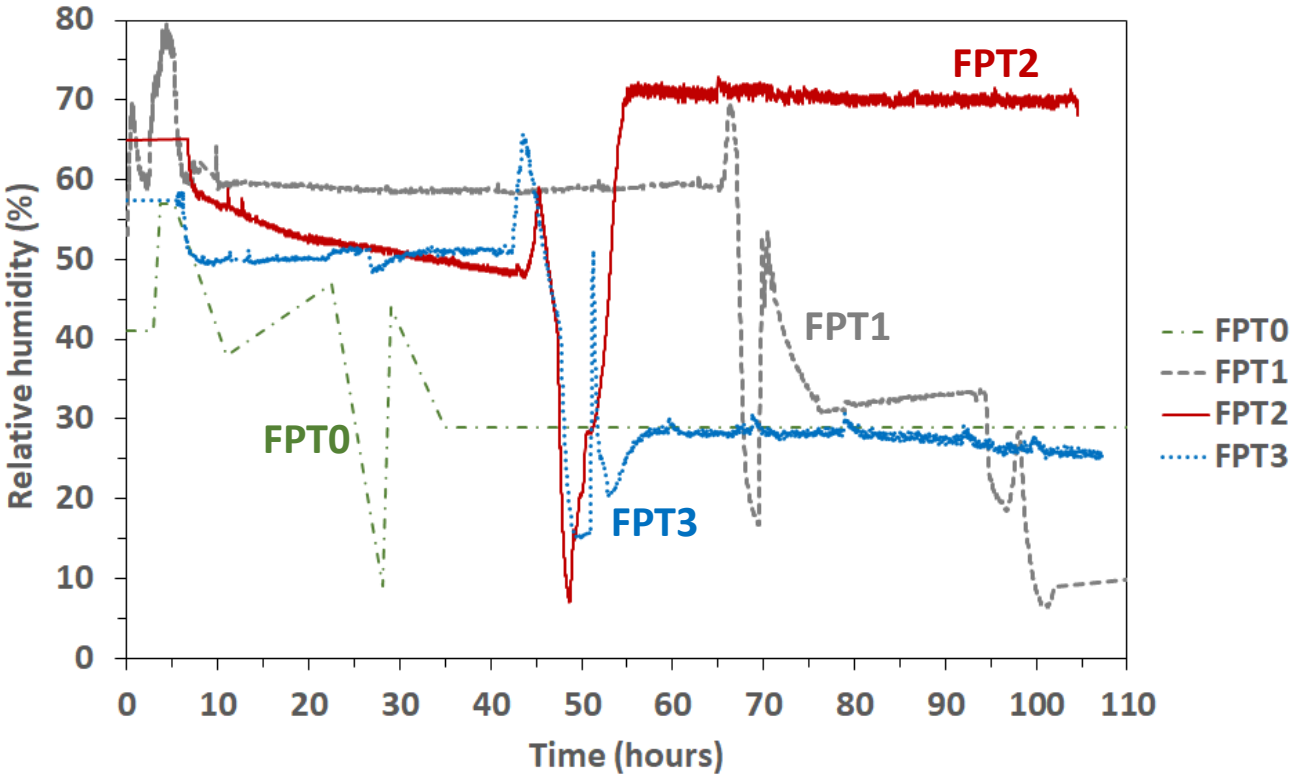

Fig. 15: Relative humidity evolution in the PHEBUS containment for FPT-0, FPT-1, FPT-2 and FPT-3 tests

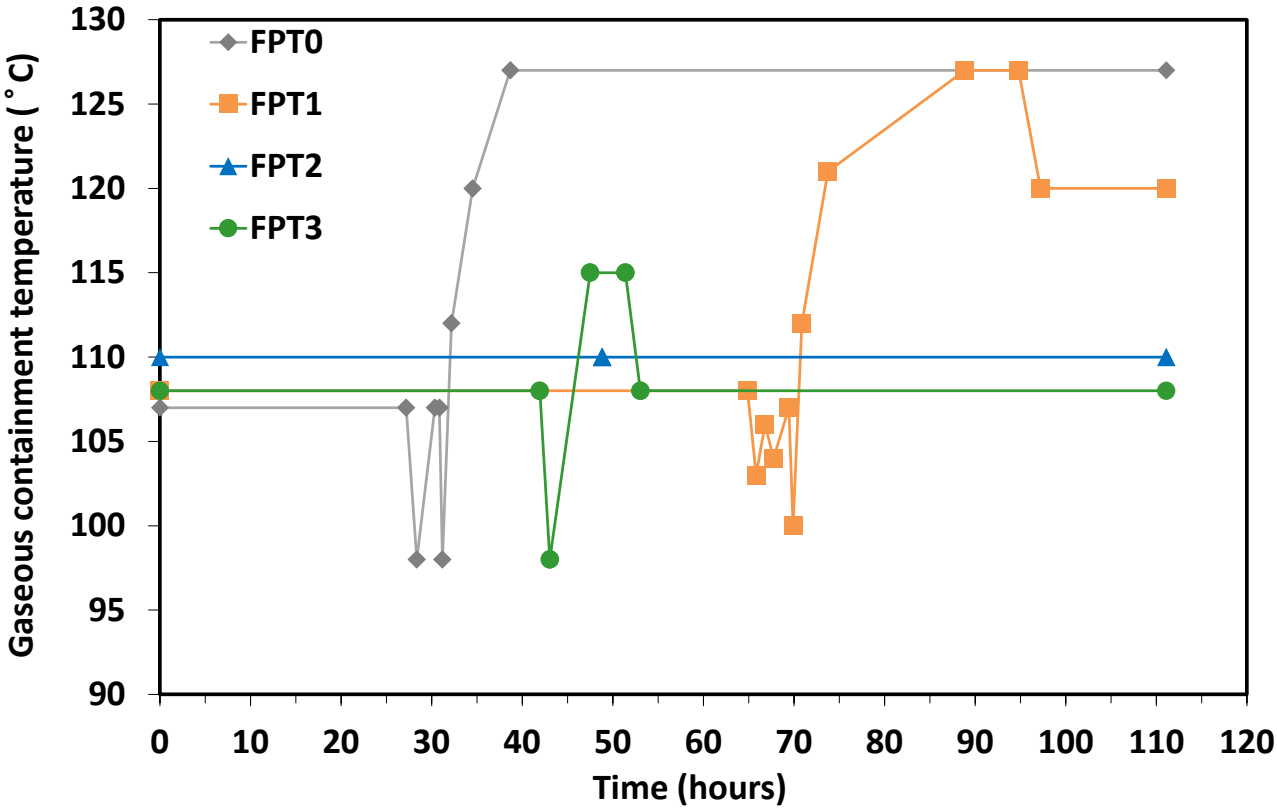

Fig. 16: Containment temperature evolution for PHEBUS FPT-0, FPT-1, FPT-2 and FPT-3 tests

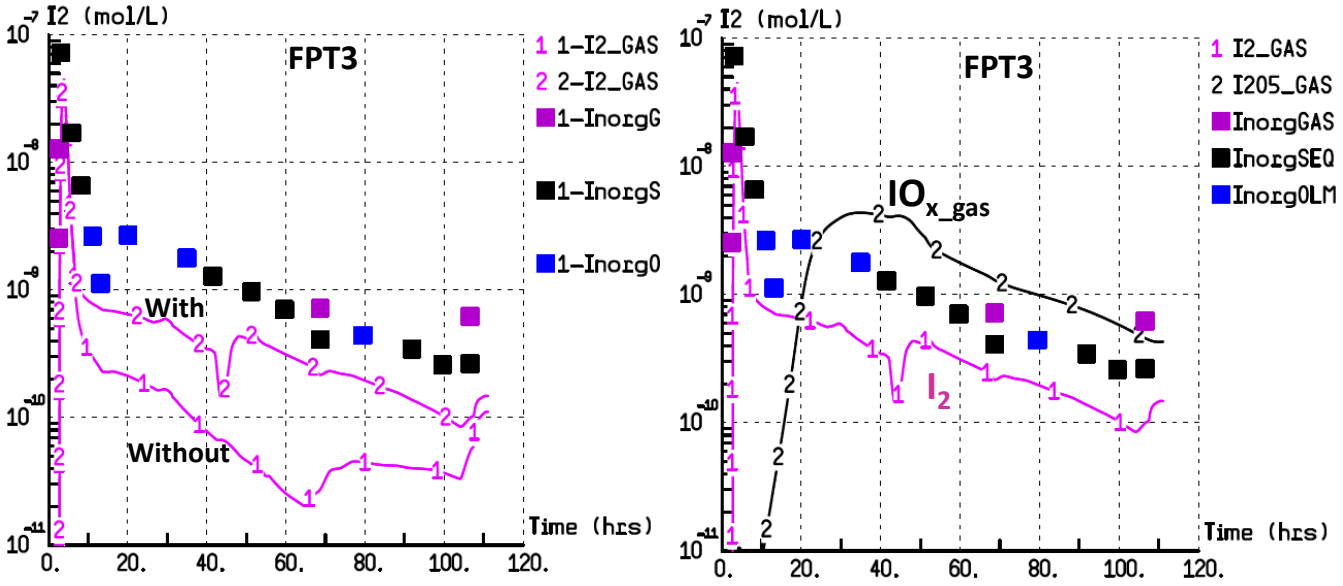

Fig. 17: Comparison of gaseous inorganic evolution without (1)/with (2) considering the IOx decomposition model (left) and comparison of the gaseous IO_{x_gas} contribution with I_2 (right) for PHEBUS FPT-3 test (InorgSEQ/InorgGAS= SEQuential Maypack whose quantification is made from a single sampling lasting tens of hundreds of seconds whereas InorgOLM/InorgO = On-Line MayPack whose measurement is based on a cumulated sampling activity since the beginning of the release)

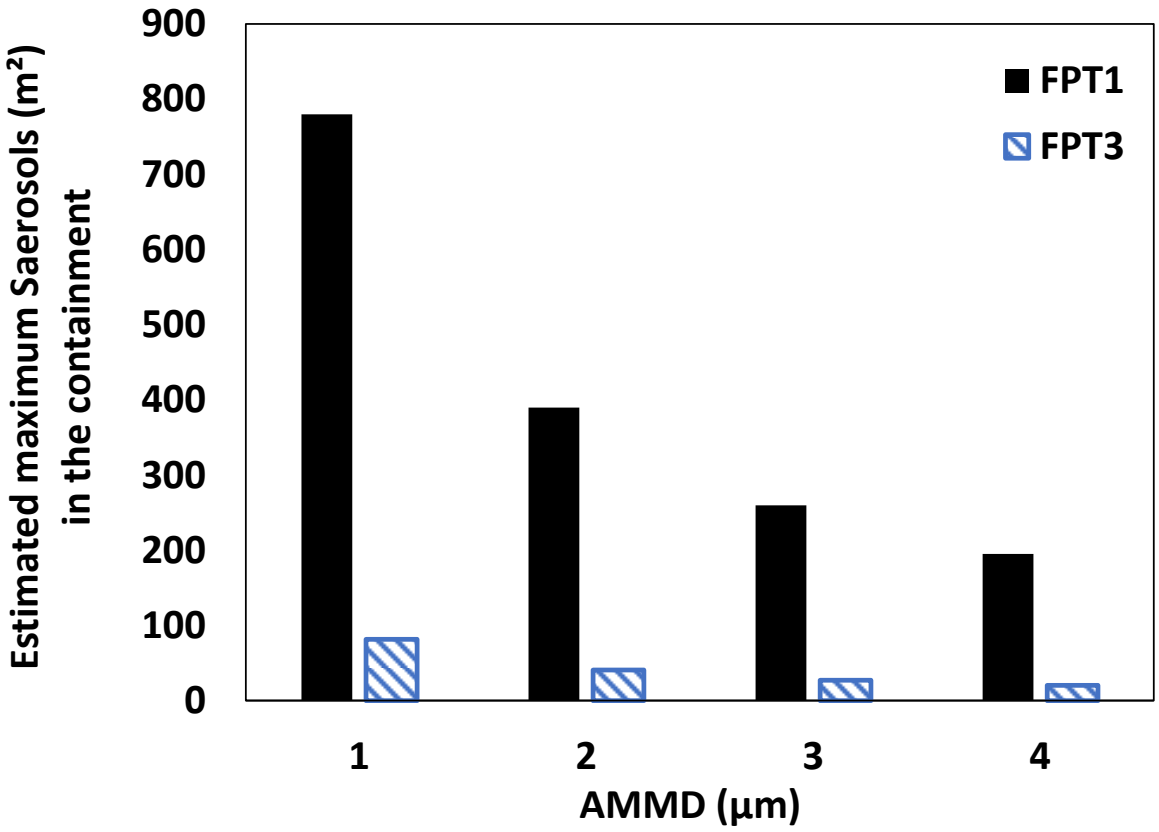

Fig. 18: maximum estimated aerosol surface in the containment versus the AMMD (assuming a density of 1 g/cm^3)

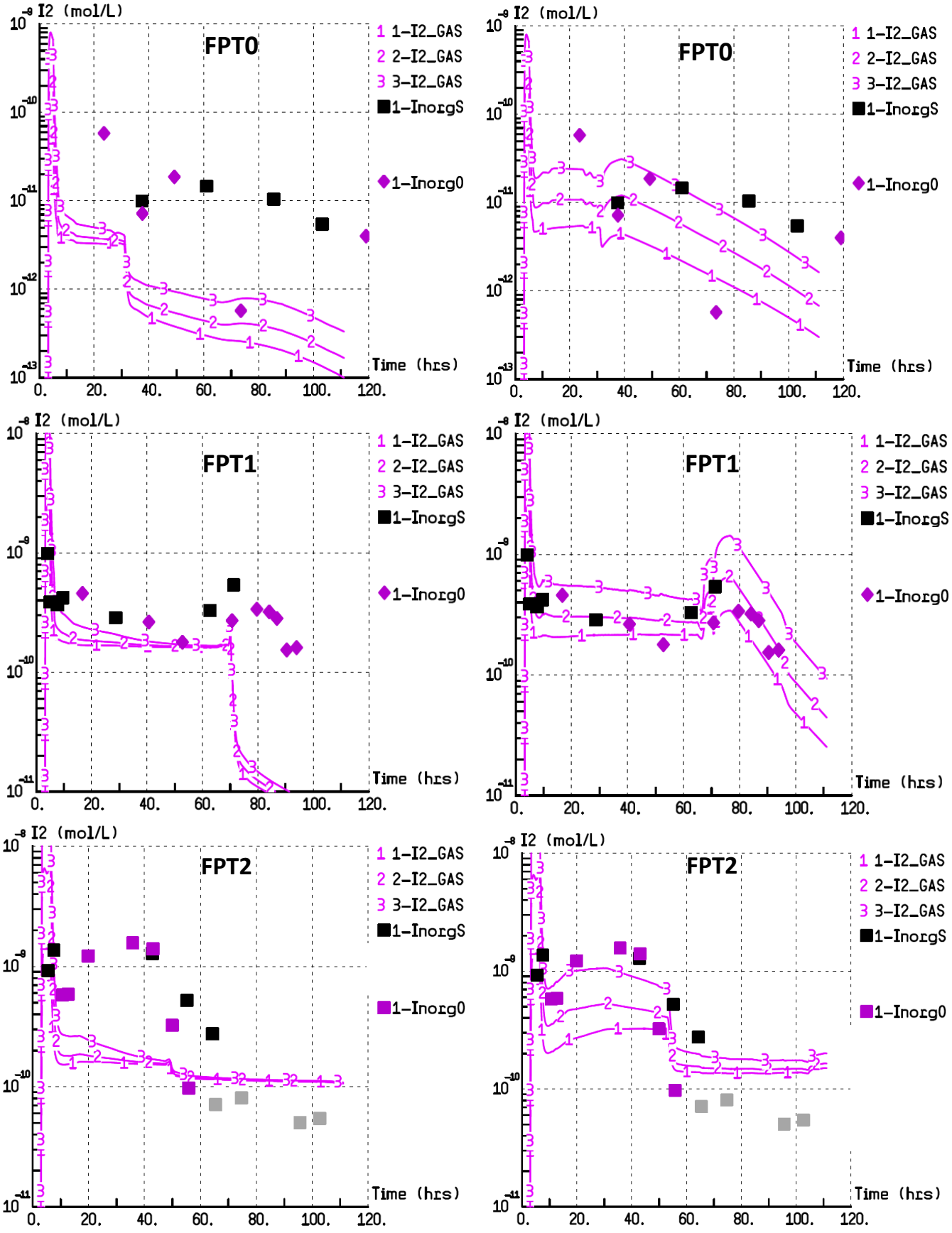

Fig. 19: Gaseous inorganic iodine evolution without considering the IOx decomposition model (left) and considering the IOx decomposition model (right) for FPT-0, FPT-1 and FPT-2) – (Curves 1, 2 and 3 correspond to a x_{I2_RCS} of respectively 2%, 10% and 30%) (InorgS = SEQuential Maypack, InorgO = On-Line MayPack)

References

1 W. G. Burns and W. R. March, "The thermal and radiolytic oxidation of aqueous I^- and the hydrolysis and disproportionation of aqueous I_2", AERE-R-10767 (1986)

2 F. Funke; P. Zeh, and al., "Radiolytic oxidation of molecular iodine in the containment atmosphere", OECD Workshop on Iodine Aspects of Severe Accident Management, Vantaa, Finland, May 18-20, 79-89 (1999)

3 C. B. Ashmore; D. J. Brown, and al., "Measurements of the radiolytic oxidation of aqueous CsI using a sparging apparatus", Nucl. Tech., 129 (3), 387-397 (2000) (https://dx.doi.org/10.13182/NT00-A3069)

4 S. Guilbert; L. Bosland, and al., "Radiolytic oxidation of iodine in the containment at high temperature and dose rate", International conference on Nuclear Energy for New Europe (NENE), September, 10-13, Portorose, Slovenia, (2007)

5 L. Bosland and J. Colombani, "Study of iodine releases from Epoxy and Polyurethane paints under irradiation and development of a new model of iodine-Epoxy paint interactions for PHEBUS and PWR severe accident applications", J. Radio. Nucl. Chem., 314 (2), 1121-1140 (2017) (https://doi.org/10.1007/s10967-017-5458-9)

6 L. Bosland; S. Dickinson, and al., "Iodine-Paint Interactions during Nuclear Reactor Severe Accidents", Annals of Nuclear Energy, 74, 184-199 (2014) (https://dx.doi.org/10.1016/j.anucene.2014.07.016)

7 S. Guilbert; L. Bosland, and al., "Formation of organic iodide in the containment in case of a severe accident", Transactions of the American Nuclear Society, Annual Meeting, June, 08 - 12 Anaheim, United States, 98, 291-292 (2008)

8 L. Bosland and J. Colombani, "Study of the radiolytic decomposition of CsI and CdI_2 aerosols deposited on stainless steel, quartz and Epoxy painted surfaces", Annals of Nuclear Energy, 141, 107241 (2020) (https://dx.doi.org/10.1016/j.anucene.2019.107241)

9 L. Bosland; O. Leroy, and al., "Study of the stability of CsI and iodine oxides (IOx) aerosols and trapping efficiency of small aerosols on sand bed and metallic filters under irradiation", Prog. Nucl. Energy., 142, 104013 (2021) (https://dx.doi.org/10.1016/j.pnucene.2021.104013)

10 B. Bartonicek and A. Habersbergerova, "Investigation of the formation possibilities of alkyl iodides in nuclear power plants", Rad. Phys. Chem., 28 (5/6), 591-600 (1986)

11 S. Dickinson; H. E. Sims, and al., "Organic iodine chemistry", Nucl. Eng. and Design, 209, 193-200 (2001) (https://dx.doi.org/10.1016/S0029-5493(01)00402-2)

12 A. K. Postma and R. W. Zadovski, "Review of Organic Iodide. Formation under Accident Conditions in Water-Cooled Reactors", United States Atomic Energy, Commission Report WASH-1233 (1972)

13 R. E. Adams; W. E. Browning, and al., "The release and adsorption of methyl iodide in the HFIR maximum credible accident", ORNL-TM-1291 (1965)

14 L. Bosland and J. Colombani, "Review of the potential sources of organic iodides in a NPP containment during a severe accident and remaining uncertainties", Annals of Nuclear Energy, 140, 107127 (2020) (https://dx.doi.org/10.1016/j.anucene.2019.107127)

15 J. H. Keller; F. A. Duce, and al., "A selective adsorbent sampling system for differentiating airborne iodine species", 11th AEC Air cleaning conference, Richland, Washington - 31st August - 03rd September (1970)

16 J. H. Keller; F. A. Duce, and al., "Hypoiodous acid: an airborne inorganic iodine species in air-steam mixtures", 11th AEC Air cleaning conference, Richland, Washington - 31st August - 03rd September (1970)

17 M. Kabat, "Testing and evaluation of absorbers for gaseous penetrative forms of radioiodine", Ontario Hdro HPD 74-8 - 13th AEC Air Cleaning conference - San Francisco, August 1974, (1974)

18 N. Hanniet and G. Repetto, "FPT-0 final report", CEA/IPSN/DRS/SEA/PEPF - Report PHEBUS PHPF IP/99/423 (1999)

19 D. Jacquemain; S. Bourdon, and al., "FPT-1 final report", CEA/IPSN/DRS/SEA/PEPF - rapport SEA 1/100 - Report PHEBUS FP IP/00/479 (2000)

20 A. C. Gregoire; P. March, and al., "FPT-2 final report", IRSN/DPAM/DIR 2008 - 272 - Report PHEBUS-FP IP/08/579 (2008)

21 F. Payot; T. Haste, and al., "FPT-3 final report", DPAM/DIR-2010-148 - PF IP/10/587 (2010)

22 F. Funke; P. Zeh, and al., "Radiolytic oxidation of molecular iodine in the containment atmosphere", OECD Workshop on Iodine Aspects of Severe Accident Management, Vantaa, Finland, May 18-20, 79-89 (1999)

23 L. Bosland; F. Funke, and al., "PARIS project: Radiolytic oxidation of molecular iodine in containment during a nuclear reactor severe accident. Part 1. Formation and destruction of air radiolysis products-Experimental results and modelling", Nucl. Eng. Des., 238 (12), 3542-3550 (2008) (https://dx.doi.org/10.1016/j.nucengdes.2008.06.023)

24 L. Bosland; F. Funke, and al., "PARIS project: Radiolytic oxidation of molecular iodine in containment during a nuclear reactor severe accident: Part 2: Formation and destruction of iodine oxides compounds under irradiation – experimental results modelling", Nucl. Eng. Des., 241 (9), 4026-4044 (2011) (https://dx.doi.org/10.1016/j.nucengdes.2011.06.015)

25 J. L. Jimenez; R. Bahreini, and al., "New particle formation from photooxidation of diiodemethane (CH_2I_2)", J. Geo. Res. Atmos., 108, 4318 (2003) (https://dx.doi.org/10.1029/2002jd002452)

26 S. Dickinson; F. Andreo, and al., "Recent advances on containment iodine chemistry ", Progress in Nuclear Energy, 52 (1), 128-135 (2010) (https://dx.doi.org/10.1016/j.pnucene.2009.09.009)

27 F. Funke; G. Langrock, and al., "Iodine oxides in large-scale THAI tests", Nucl. Eng. & Des., 245, 206-222 (2012) (https://dx.doi.org/10.1016/j.nucengdes.2012.01.005)

28 B. R'mili; R. Strekowski, and al., "Important effects of relative humidity on the formation processes of iodine oxide particles from CH_3I photo-oxidation", J. Hazardous Material, 433, 128729 (2022) (https://dx.doi.org/10.1016/j.jhazmat.2022.128729)

29 S. Zhang, "Etudes cinétiques de l'oxydation radicalaire en phase gazeuse d'iodures organiques et de la formation de particules d'oxydes d'iode sous conditions simulées de l'enceinte d'un réacteur nucléaire en situation d'accident grave", PhD - Université Aix-Marseille, France (2012)

30 R. Atkinson; D. L. Baulch, and al., "Evaluated kinetic and photochemical data for atmospheric chemistry: Volume III - gas phase reactions of inorganic halogens", Atmos. Chem. Phys., 7, 981-1191 (2007) (https://dx.doi.org/10.5194/acp-7-981-2007)

31 N. Girault; L. Bosland, and al., "LWR severe accident simulation: iodine behaviour in FPT2 experiment and advances on containment iodine chemistry", Nucl. Eng. Des., 243, 371-392 (2012) (https://dx.doi.org/10.1016/j.nucengdes.2011.11.011)

32 O. Leroy and L. Bosland, "Study of the stability of iodine oxides (IxOy) aerosols in severe accident conditions", Annals of Nucl. En., 181, 109526 (2023) (https://dx.doi.org/10.1016/j.anucene.2022.109526)

33 J. P. Van Dorsselaere; P. Chatelard, and al., "Validation Status of the ASTEC Integral Code for Severe Accident Simulation", Nucl. Tech., 170 (3), 397-415 (2010) (https://dx.doi.org/10.13182/NT10-A10326)

34 L. Cantrel; F. Cousin, and al., "ASTEC V2 severe accident integral code: Fission product modelling and validation", Nucl. Eng. & Des., 272, 195-206 (2014) (https://dx.doi.org/10.1016/j.nucengdes.2014.01.011)

35 P. Chatelard; S. Belon, and al., "Main modelling features of ASTEC V2.1 major version", Annals of Nuclear Energy, 93, 83-93 (2016) (https://dx.doi.org/10.1016/j.anucene.2015.12.026)

36 C. Mun; L. Bosland, and al., "OECD-STEM Project and its Follow-up STEM2", Proc. of the Int. OECD-NEA/NUGENIA-SARNET Workshop on the Prog. in Iodine Behaviour for NPP Acc. Anal. and Manag. - March 30, April 1 - Marseille (France), Paper 1-10, (2015)

37 M. W. Chase, "NIST-JANAF Themochemical Tables, Fourth Edition", J. Phys. Chem. Ref. Data, Monograph 9, (1998)

38 D. K. Smith; M. L. Pantoya, and al., "The water-iodine oxide system: a revised mechanism of hydration and dehydration", RSC Adv., 7, 10183-10191 (2017) (https://dx.doi.org/10.1039/c6ra27854j)

39 C. Farley and M. L. Pantoya, "Reaction kinetics of nanometric aluminum and iodine pentoxide", J. Therm. Anal. Calorim., 102, 609-613 (2010) (https://dx.doi.org/10.1007/s10973-010-0915-5)

40 H. Fjellvag and A. Kjekshus, "The crystal structure of I_2O_4 and its relations to other Iodine-oxygen containing compounds", Acta Chemica Scandinavia, 48, 815-822 (1994) (https://dx.doi.org/10.1002/chin.199509004)

41 G. Daehlie and A. Kjekshus, "Iodine oxides. Part I. On I_2O_3-SO_3, I_2O_3-4SO_3-H_2O, I_2O_3-SeO_3 and I_2O_4", Acta Chemica Scandinavia, 18, 144-156 (1964)

42 K. Selte and A. Kjekshus, "Iodine oxides. Part II. On the system H_2O-I_2O_5", Acta Chemica Scandinavia, 22, 3309-3320 (1968)

43 T. Wu; A. Sybing, and al., "Aerosol synthesis of phase pure iodine/iodic biocide microparticles", J. Mat. Res., 32 (4), 890-896 (2017) (https://dx.doi.org/10.1557/jmr.2017.6)

44 A. Kokesnikov; A. Krishnamoorthy, and al., "Inelastic Neutron Scattering Study of Phonon Density of States of Iodine Oxides and First-Principles Calculations", J. Phys. Chem. Lett., 14, 10080-10087 (2023) (https://doi.org/10.1021/acs.jpclett.3c02357)

45 C. M. Stevens and L. Krout, "Method for the determination of the concentration and of the carbon and oxygen isotopic composition of atmospheric carbon monoxide", Int. J. Mass Spect. & Ion Phys., 8, 265-275 (1972) (https://dx.doi.org/10.1016/0020-7381(72)83017-1)

46 K. A. Rao; K. K. Pushpa, and al., "Estimation of carbon monoxide and carbon dioxide at sub-ppm level concentrations in ammonia synthesis gas", J. Chromat. Sci., 169, 306-310 (1978) (https://dx.doi.org/10.1093/chromsci/16.7.306)

47 H. J. Kavanaugh; J. W. Dahlby, and al., "The gravimetric determination of carbon in uranium-plutonium carbide materials", LA-7981 - Los Alamos Scientific Laboratory (1980)

48 G. Kainz and F. Scheidl, "Neue Ergebnisse über die Reaktionsvorgänge bei der Sauerstoffbestimmung", Mikrochimica acta, 54 (4-5), 624-633 (1966) (https://dx.doi.org/10.1007/BF01222985)

49 B. K. Little; S. B. Emery, and al., "Physiochemical characterization of Iodine(V) oxide, Part 1: hydration rates", Propellants Explos. Pyrotech., 35, 1-10 (2010) (https://dx.doi.org/10.1002/prep.201400225)

50 J. C. Gomez-Martin; T. R. Lewis, and al., "Insights into the Chemistry of Iodine New Particle Formation: The Role of Iodine Oxides and the Source of Iodic Acid", J. Am. Chem. Soc., 144, 9240-9253 (2022) (https://doi.org/10.1021/jacs.1c12957)

51 J. Trincal, "Modélisation du comportement de l'iode dans l'atmosphère", PhD - Université de Lille 1, France (2015)

52 A. Saiz-Lopez; J. M. C. Plane, and al., "Atmospheric chemistry of iodine", Chemical Reviews, 112, 17773-11804 (2012) (https://dx.doi.org/dx.doi.org/10.1021/cr200029u)

53 G. Glowa; C. J. Moore, and al., "The main outcomes of the OECD Behaviour of Iodine (BIP) Project", Annals of Nuclear Energy, 61, 179-189 (2013) (https://dx.doi.org/10.1016/j.anucene.2013.02.036)

54 L. Bosland and J. Colombani, "Review of the potential sources of organic iodides in a NPP containment during a severe accident and remaining uncertainties", Annals of Nuclear Energy, 140, 107127 (2020) (https://dx.doi.org/10.1016/j.anucene.2019.107127)

55 L. Bosland; G. Weber, and al., "Modeling and interpretation of iodine behavior in PHEBUS FPT-1 containment with ASTEC and COCOSYS codes", Nucl. Tech., 177 (1), 36-62 (2012) (https://dx.doi.org/10.13182/NT12-A13326)

56 L. Bosland; L. Cantrel, and al., "Evaluation of the dose rate inhomogeneities in PHEBUS containment during FPT1 and FPT3 tests", 31th CCIC meeting, March 23rd, JRC PETTEN, (2010)

57 N. Girault; L. Bosland, and al., "LWR severe accident simulation fission product behavior in FPT-2 experiment", Nucl. Tech., 169 (3), 218-238 (2010) (https://dx.doi.org/10.13182/NT10-A9375)

58 S. Gupta; E. Schmidt, and al., "THAI test facility for experimental research on hydrogen and fission product behaviour in light water reactor containments", Nucl. Eng. Des., 294, 183-201 (2015) (http://dx.doi.org/10.1016/j.nucengdes.2015.09.013)

59 S. Gupta; G. Poss, and al., "Aerosol and Iodine Issues, and Hydrogen Mitigation under Accidental Conditions in Water-cooled Reactors - Thermal-hydraulics, Hydrogen, Aerosols and Iodine (THAI-2) Project - Final report", OECD-NEA/CSNI/R(2016)8 (2017)

60 E. C. Beahm; C. F. Weber, and al., "Iodine chemical forms in LWR severe accidents", ORNL/TM-11861 - NUREG/CR-5732 (1991)

61 L. Soffer, "Accident Source Terms for Light-Water Nuclear Power Plants.", NUREG-1465, U.S. Nuclear Regulatory Commission (1995)

62 D. Manesse; A. Fallot, and al., "Réévaluation des termes-sources de référence des REP - Note de synthèse", IPSN/DPEA/SEAC/2000 - 036 (2000)

63 F. Funke, "Data analysis and modelling of organic iodide production at painted surfaces", OECD Workshop on Iodine Aspects of Severe Accident Management, Vantaa, Finland, May 18-20, 151-168 (1999)

64 F. Funke; S. Gupta, and al., "Interaction of gaseous I_2 with painted surfaces and aerosols in large-scale THAI tests", Proc. of the Int. OECD-NEA/NUGENIA-SARNET Workshop on the Prog. in Iodine Behaviour for NPP Acc. Anal. and Manag. - March 30, April 1 - Marseille (France), (2015)

65 A. Zoulalian and E. Belval-Haltier, "Interaction between molecular iodine in a gas phase and paints aged in a nuclear power plant", Nucl. Tech., 130, 362-371 (2000) (https://dx.doi.org/10.13182/NT00-A3099)

66 T. Nugraha, "Interactions of I_2 with paints under condensing steam conditions", PhD - University of Toronto, Canada (2003)

67 L. F. Parsly, "Design Considerations of Reactor Containment Spray Systems. Part IV, Calculation of Iodine-Water Partition Coefficients", ORNL/TM-2412 (1970)

68 R. K. Hilliard; A. K. Postma, and al., "Removal of Iodine and particules by sprays in the containment systems experiments", Nucl. Tech., 10, 499-519 (1971)

69 B. Clement; L. Cantrel, and al., "State of the art report on iodine chemistry", OECD-NEA-CSNI-R(2007)1 (2007)

70 F. Funke; P. Zeh*, and al.*, "Radiolytic oxidation of molecular iodine in the containment atmosphere", OECD Workshop on Iodine Aspects of Severe Accident Management, Vantaa, Finland, May 18-20, 79-89 (1999)

71 A. C. Vikis and R. Macfarlane, "Reaction of iodine with ozone in the gas phase", J. Phys. Chem, 89, 812-815 (1985) (https://dx.doi.org/10.1021/j100251a019)

72 L. Bosland and K. Chevalier-Jabet, "Main lessons learnt from 40 years of R&D on iodine source term prediction: Identification of the main parameters governing iodine volatility in PHEBUS FP tests", Prog. Nucl. Energy., 177, 105473 (2024) (https://dx.doi.org/10.1016/j.pnucene.2024.105473)